Pressure-induced polymerization of polycyclic arene-perfluoroarene co-crystals: Single crystal X-ray diffraction studies, reaction kinetics, and design of columnar hydrofluorocarbons

Alexandra Friedrich,[a]* Ines E. Collings,[b] Kamil Dziubek,[c] Samuele Fanetti,[c,d] Krzysztof Radacki,[a] Javier Ruiz-Fuertes,[e,f] Julio Pellicer-Porres,[e] Michael Hanfland,[b] Daniel Sieh,[a] Roberto Bini,[c,d,g]* Stewart J. Clark,[h]* Todd B. Marder [a]*

[a] Institut für Anorganische Chemie, Julius-Maximilians-Universität Würzburg, Am Hubland, 97074 Würzburg, Germany

[b] European Synchrotron Radiation Facility, 71 Avenue des Martyrs, 38000 Grenoble, France

[c] LENS, European Laboratory for Nonlinear Spectroscopy, Via Nello Carrara 1, 50019 Sesto Fiorentino (FI), Italy

[d] ICCOM-CNR, Institute of Chemistry of OrganoMetallic Compounds, National Research Council of Italy, Via Madonna del Piano 10, I-50019 Sesto Fiorentino, Firenze, Italy

[e] MALTA Consolider Team, Dpto. Física Aplicada-ICMUV, Universitat de València, C/ Doctor Moliner 50, 46100 Burjassot, Spain

[f] DCITIMAC, MALTA Consolider Team, Universidad de Cantabria, 39005 Santander, Spain

[g] Dipartimento di Chimica "Ugo Schiff" dell'Università degli Studi di Firenze, Via della Lastruccia 3, 50019 Sesto Fiorentino (FI), Italy

[h] Department of Physics, University of Durham, Science Labs, South Road, Durham DH1 3LE, UK

ABSTRACT: Pressure-induced polymerization of aromatic compounds leads to novel materials containing sp^3 carbon-bonded networks. The choice of the molecular species and the control of their arrangement in the crystal structures via intermolecular interactions such as the arene-perfluoroarene interaction, can enable the design of target polymers. We have investigated the crystal structure compression and pressure-induced polymerization reaction kinetics of two polycyclic 1:1 arene-perfluoroarene co-crystals, naphthalene:octafluoronaphthalene (**NOFN**) and anthracene:octafluoronaphthalene (**AOFN**), up to 25 and 30 GPa, respectively, using single-crystal synchrotron X-ray diffraction, infrared spectroscopy, and theoretical computations based on density-functional theory. Our study

shows the remarkable pressure stability of the parallel arene-perfluoroarene π-stacking arrangement and a reduction of the interplanar π-stacking separations by ca. 19–22 % before the critical reaction distance is reached. A further strong, discontinuous, and irreversible reduction along the stacking direction at 20 GPa in **NOFN** (18.8 %) and 25 GPa in **AOFN** (8.7 %) indicates the pressure-induced breakdown of π–stacking by formation of σ-bonded polymers. The association of the structural distortion with the occurrence of a chemical reaction is confirmed by a high-pressure kinetic study using infrared spectroscopy, indicating a one-dimensional polymer growth. Structural predictions for the fully polymerized high-pressure phases consisting of highly ordered rods of hydrofluorocarbons, are presented based on theoretical computations, which are in excellent agreement with the experimentally determined unit cell parameters. We show that the polymerization takes place along the arene–perfluoroarene π–stacking direction and that the lateral extension of the columns depends on the extension of the arene and perfluoroarene molecules.

INTRODUCTION

Pressure-induced polymerization (PIP) of aromatic hydrocarbons is an intensely studied topic due to interest in the generation of novel carbon nanostructures of high density.[1] While there is a general consensus on the breakdown of aromaticity and changes in carbon hybridization from sp^2 to sp^3 upon reaction, which usually takes place in the pressure range between 15–35 GPa for aromatic hydrocarbons,[2] the mechanism of the polymerization reaction is still not well understood. Comprehension of the process would very much enhance the possibility of controlling the structure and, hence, properties of the resulting nanostructures. The first indirect observations indicating PIP in aromatic hydrocarbons were reported as early as 1964, 1967 and 1970.[2a, 3] By far the most studied aromatic compound at high pressure, and with respect to PIP, is benzene.[1a, 1b, 2d, 2f, 4] Similar onset pressures for PIP were observed for benzene (20–23 GPa),[1b, 2f, 4f, 4g] anthracene (22 GPa),[2b, 5] and naphthalene (between 15 and 20 GPa).[2c] In most cases, the polymerization processes have been studied via spectroscopic methods such as IR and Raman spectroscopy, which confirm the hybridization change from Csp^2 to Csp^3, or powder X-ray diffraction which, however, is usually limited to determining unit-cell parameters of a molecular precursor and, most often, only shows the amorphization process upon reaction, without further information on the structure of the polymerized phase. Detailed information on the possible crystal structures and mechanisms of the

polymerization has been obtained mainly from theoretical studies,[1, 2d, 4b, 6] while experimental evidence is rare, a breakthrough being the detailed analysis of the pressure-quenched benzene-derived carbon nanothread by Fitzgibbons *et al*.[1b] Detailed studies on new polyaniline and carbon nitride nanothreads formed from C/H/N aromatic compounds appeared recently.[7] PIP mechanisms and models for the polymers were also proposed for 1:1 arene:perfluoroarene co-crystals of benzene:hexafluorobenzene ($C_6H_6{\cdot}C_6F_6$),[8] and, during the preparation of our manuscript, of naphthalene:octafluoronaphthalene (**NOFN**, $C_{10}H_8{\cdot}C_{10}F_8$), one of the two compounds studied here.[9] For the latter one, only unit cell parameters of the low-pressure phase were reported from single-crystal X-ray diffraction; no atom positions or complete unit cell parameters of the polymerized phase were presented.

A critical intermolecular nearest-neighbor C···C distance of 2.6 Å, corrected by a thermal translational contribution using the maximum of the phonon density of states, was computed for the onset of pressure-induced polymerization in benzene.[1a] This distance was also proposed to be critical based on reflection positions of powder X-ray diffraction data of phenanthrene at pressures up to 25 GPa.[10] Almost the same critical C···N and C···C reaction distance (2.5 Å) was found for *s*-triazine and aniline, respectively, from thermally corrected powder X-ray diffraction data.[11] For the benzene-hexafluorobenzene co-crystal, a nearest-neighbor C···C distance of 2.8 Å with thermal uncertainty was observed from powder neutron diffraction data before the onset of polymerization.[8] Recently, the crystal structure of melamine, $C_3H_6N_6$, was reported up to 36 GPa at which a reversible phase transition takes place, while amorphization was reported at a much higher pressure of 45 GPa.[12] The stability of melamine to such a high pressure was attributed to the stability of the hydrogen bonds.[12] Another study reported the influence of incorporation of helium, which acted as pressure-transmitting medium, on the molecular packing and crystal structure compression of 4-hydroxycyanobenzene up to 26 GPa.[13]

Herein, we take a new approach by studying not only the development of the unit-cell parameters, but also of the intra- and intermolecular distances, at a high level of accuracy, as a function of increasing pressure close to and through the polymerization reaction using single-crystal X-ray diffraction. Changes in the intermolecular and C···C bond distances just before the reaction should give the most accurate information on the polymerization process and loss of aromaticity.[14] To the best of our knowledge, no other single-crystal structure data on polycyclic aromatic hydrocarbons (PAHs) or related

compounds have yet been reported at pressures above 10 GPa and close to the onset of polymerization. Our experimental results are complemented by theoretical computations[15] based on density functional theory (DFT) studies of the crystal structures in the solid state in order to obtain information on the structure of the polymerized high-pressure phase, and by high-pressure infrared spectroscopic studies to obtain the kinetics of the polymerization reaction.

We focus on the effect of pressure on the arene-perfluoroarene π–π stacking interaction in 1:1 co-crystals of PAHs with polycyclic aromatic fluorocarbons. In contrast to the pure aromatic hydrocarbons, these co-crystals generally form highly oriented, π-stacked systems due to the attractive multipole as well as dispersion forces between aromatic and highly fluorinated aromatic components, making the arene-perfluoroarene interaction a robust supramolecular synthon.[16] The attractive interaction results from opposite multipoles (often approximated as quadrupole moments) due to the difference in polarization of the C–H versus the C–F bonds as a consequence of the different relative electronegativities of hydrogen and fluorine atoms with respect to the carbon atoms. This results in a face-to-face association in contrast to the edge-to-face stacking (herringbone-type) of pure aromatic or perfluoroaromatic molecules (Figure 1).[16d, 17] The strength and effects of this interaction type were discovered by Patrick and Prosser in 1960, by the formation and analysis of a 1:1 co-crystal of benzene and hexafluorobenzene.[18] Common structural features of arene-perfluoroarene complexes, which include an offset molecular overlap, parallelism of planes, and the formation of alternating stacks of fluorinated and non-fluorinated arenes with mean inter-planar distances varying from 3.39 to 3.56 Å, were described by Dahl for the first time.[16a] The geometrical parameters of the molecular stacks with respect to the stacking axis, described in detail by Marder and co-workers,[16d] are illustrated in Figures 1 and S8. Marder and co-workers have used this type of interaction in crystal engineering of various co-crystals[16d, 19] including, among many others, 1:1 co-crystals of anthracene and octafluoronaphthalene (**AOFN**, $C_{14}H_{10}{\cdot}C_{10}F_8$).[16d] Very recently, interest in the high-pressure behavior and pressure-induced polymerization of arene–perfluoroarene co-crystals has emerged, as the co-crystals serve as valuable precursors for the formation of C/H/F polymers.

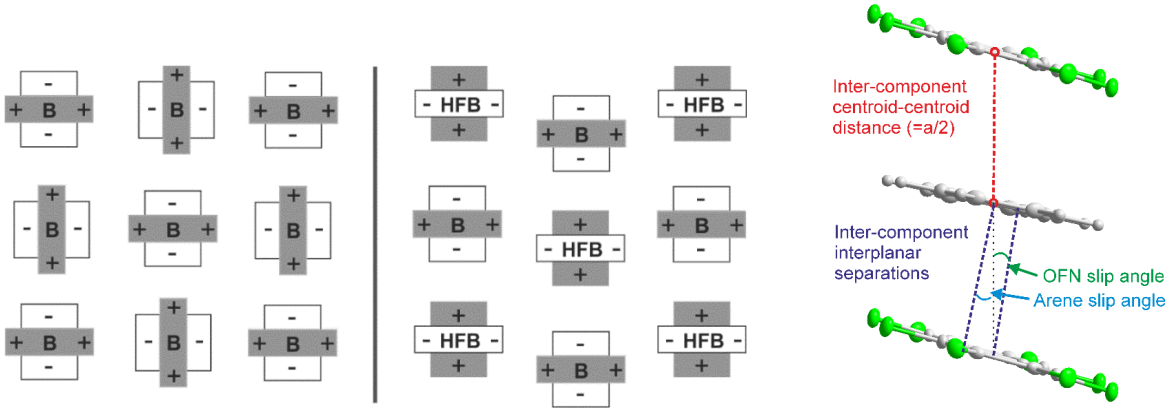

Figure 1. Schematic representation of (left) the herringbone packing of benzene (B) in the solid state and (middle) the stacked arrangement of the benzene (B)-hexafluorobenzene (HFB) co-crystal (based on that of Williams[17]). Right: Schematic of the arene–perfluoroarene stack in naphthalene:octafluoronaphthalene (**NOFN**) showing the definition of the intermolecular parameters after Marder and co-workers.[12p] The interplanar separation is calculated using a vertical line between the centroid of one molecule and its intersection point with the mean plane through the other molecule. The difference between the centroid-centroid distances and the interplanar separations of the respective molecules depends on the inclination of the normal direction of the molecular plane with respect to the stacking axis, which is the *a* axis in **NOFN** and **AOFN** (anthracene:octafluoronaphthalene), and this is represented by the value of the slip angle.

Ma and co-workers studied the pressure-accelerated cycloaddition of azides and alkynes with the functional groups pre-organized *via* arene-perfluoroarene interactions.[20] A Raman-spectroscopic study on a 1:1 co-crystal of naphthalene and octafluoronaphthalene (**NOFN**) up to 8 GPa revealed its stability in this pressure range pointing to a robust structural arrangement of the stacking at high pressure.[21] The stability of the crystal structure of **NOFN** and, hence, the arene-perfluoroarene stacking arrangement up to polymerization pressure at 20 GPa was reported recently from unit cell parameters obtained by single-crystal X-ray diffraction and from IR spectroscopy.[9] Single-crystalline order was even noted in the polymer phase of **NOFN**, even if crystal structural information could not be extracted in that study. From theoretical calculations, the authors proposed a [4+2] cycloaddition model proceeding along the stacking axis of the molecules as a strong candidate for the polymerization mechanism leading to polymerized rods with single-crystalline order.[9] In contrast, aromatic compounds with herringbone-type molecular arrangement often show pressure-induced phase transitions leading to more parallel arrangements of the molecules in their crystals, examples being

phenanthrene and pyrrole.[10, 22] However, the smallest arene-perfluoroarene system, i.e., the 1:1 co-crystal of benzene and hexafluorobenzene, shows a very complicated behavior at high pressure, i.e., four high-pressure phase transitions at < 12 GPa and a final pressure-induced polymerization above 25 GPa.[2e, 8] The main focus of those studies was the comparison of the PIP of pure benzene or hexafluorobenzene[23] with that of the co-crystal, especially as the latter leads to a pre-organization of the column structure *via* arene-perfluoroarene interactions. This could lead to the generation of ordered carbon nanostructures upon PIP. Due to its complex high-pressure behavior, only the crystal structure of the first high-pressure polymorph, phase V, could be determined from single-crystal X-ray diffraction at 1 GPa, while the structures of the other phases were determined from time-of-flight neutron powder diffraction in a more recent study.[2e, 8] Interestingly, the authors proposed the formation of H-F graphane with a layered structure *via* pressure-induced Diels-Alder reactions, and not a columnar polymer, as the end product of the pressure-induced chemical reactions.[8]

In our study, we report the single-crystal structures of two arene-perfluoroarene co-crystals, i.e., naphthalene-octafluoronaphthalene (**NOFN**) and anthracene-octafluoronaphthalene (**AOFN**), at pressures up to the polymerization reactions (19 and 25 GPa, respectively) in order to gain insight into the evolution, stability, and strength of the arene-perfluoroarene interaction at high pressure and to obtain accurate structural parameters at pressures close to that of the polymerization reaction. Experimentally determined crystal structures are compared to crystal structures computed using DFT. From our high-quality structural data, and the evolution of the unit cell parameters of **NOFN** and **AOFN** across the polymerization-induced reaction and of **AOFN** on decompression, and our DFT calculations, we propose a structural model for the fully-polymerized high-pressure phases. Our results on **NOFN** are compared with the recently published polymerization models for **NOFN** and our structural and theoretical data confirm the proposed polymerization mechanism. We also present the kinetics of the polymerization reaction at high pressure from infrared (IR) spectroscopic studies, and confirm the one-dimensionality of the polymerization mechanism in both **NOFN** and **AOFN**.[24] Thus, we report herein: (1) a deep insight into the PIP of **NOFN** and **AOFN**; (2) atom positions of the compressed structures of both **NOFN** and **AOFN;** (3) accurate anisotropic displacement parameters for **NOFN**, up to a pressure close to the reaction onset; (4) theoretically computed crystal structures of the low-pressure phase of **AOFN** between 1 and 100 GPa and of **NOFN** between 2 and 40 GPa; (5) experimentally

determined unit cell parameters of the polymerized high-pressure phases; (6) theoretically computed structural models of the polymers of **AOFN** between 1 and 100 GPa and of **NOFN** between 2 and 40 GPa which are in agreement with experimental unit cells; (7) the evolution of the IR active vibrational modes at pressures up to the reaction onset; (8) a kinetic study of the chemical reactions using IR spectroscopy; and (9) the computed IR frequencies and intensities for both low- and high-pressure phases of **NOFN** and **AOFN**.

RESULTS AND DISCUSSION

Unit-cell compression before and through the polymerization process from single-crystal X-ray diffraction data

As observed in many aromatic or molecular compounds,[25] the unit cells of both **AOFN** and **NOFN** are strongly compressed in the lower pressure region (0–2.5 GPa) before increased intermolecular repulsion becomes responsible for the decrease of the compression rate (Figure 2, Tables S1 and S2). Continuous compression of the unit cell is observed up to 19–20 GPa for **NOFN** and 23–25 GPa for **AOFN**. At higher pressures, a strong and discontinuous reduction of the unit-cell volume by -11 and -7 % for **NOFN** and **AOFN**, respectively, indicates the occurrence of a reconstructive phase transition or chemical reaction. This is associated with a significant decrease of the diffraction quality and, hence, increase of the mosaicity of the crystals, which is more severe in **NOFN** due to the larger volume reduction, indicating major structural changes in both compounds. Note the use of helium as the pressure-transmitting medium, which still provides quasi-hydrostatic conditions at the highest pressures of our experiments.[26] In **NOFN,** the crystal quality starts to decrease at 18.9(1) GPa and, at 20.6(3) GPa, both the low- and the high-pressure phases co-exist. However, single-crystal reflections of both phases are already very broad and, at a higher pressure of 22.5(3) GPa, only very weak and broad scattering by the high-pressure phase is observed (Figure S1). These observations are consistent with the reported polymerization pressure of 20 GPa and the observed decrease of single-crystal quality of **NOFN** by Ward *et al*.[9] In contrast to Ward *et al*., we were able to index the reflections of the high-pressure phase of **NOFN** and obtain the unit cell parameters from the diffraction data of both of the crystals loaded at 20.6(3) GPa (Tables 1 and S3). Importantly, the single-crystal reflections of **AOFN** remained relatively sharp through the phase transition, although they were of much lower intensity,

and the quality of the **AOFN** crystal did not further decrease upon increasing the pressure to 29 GPa (Figure S2). This allowed us to index the reflections of the high-pressure phase and to follow the pressure evolution of its unit-cell parameters (Figure 2, Tables 1 and S4). Unfortunately, the intensities of the reflections were too weak to allow full solution of the crystal structures of the high-pressure phases as there were only a few strong unique reflections with intensity > 4σ, significantly less than the number of parameters to be optimized during crystal structure refinement. The low intensities of the single-crystal reflections of the high-pressure phases and the increase in mosaicity may be explained by strongly disordered structures, large changes in the crystal structure due to a strong rearrangement of the molecules or the formation and/or breaking of chemical bonds, or by the formation of highly ordered nanomaterials which produce broad reflections due to the small number of coherently diffracting unit cells. This interpretation is consistent with recent high-resolution transmission electron microscopy studies on nanothread crystals of polymerized benzene and aniline synthesized at high pressure and temperature, which revealed bends and defects in the nanocrystals contributing to the broadening of diffraction spots.[4t, 7a] The formation of nanomaterials is supported by the fact that the material in the high-pressure phase after recovery appeared to be a powder rather than a single crystal. However, we did not observe amorphization in the pressure range investigated.

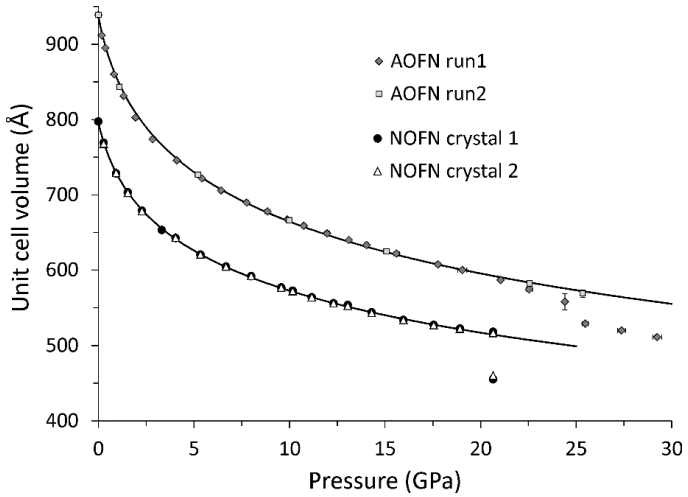

Figure 2. Compression of the unit-cell volumes of **AOFN** and **NOFN** obtained from single-crystal X-ray diffraction data. At 20.6(3) GPa, a volume reduction of -11 % is observed in **NOFN**, while in **AOFN** a volume reduction of -7 % is observed between 23 and 25.5 GPa. Lines represent 3rd-order Vinet[27] equation of state fits to the p–V data, which result in the bulk moduli B = 7.2(2) GPa and 7.1(1) GPa, and their pressure

derivatives $B' = 8.6(1)$ and 9.25(8) for **AOFN** ($V_0 = 936(1)$ Å³) and **NOFN** ($V_0 = 795.9(7)$ Å³), respectively.

Table 1: Unit-cell parameters of the high-pressure phases of NOFN and AOFN obtained from single-crystal X-ray diffraction data and from DFT calculations on the polymerized high-pressure structures.

	NOFN (HP-phase)		**AOFN** (HP-phase)	
	Experiment	Theory	Experiment	Theory
Pressure / GPa	20.7(3)	20	29.2(2)	30
a / Å	4.858(4)	4.7311	4.821 (2)	4.3764
b / Å	8.089(3)	8.2669	16.12(3)	17.2126
c / Å	11.77(3)	12.0693	6.740(3)	6.7564
α / °	90	90	90	90
β / °	100.0(2)	106.46	102.84(5)	98.84
γ / °	90	90	90	90
Volume / Å^3	455(1)	452.71	511(1)	502.90

The strongest compression of the unit cells of both **NOFN** and **AOFN** low-pressure phases proceeds along the *a* axis, which is the π-stacking direction (Figure 3). Moderate compression is observed along the *c* axis and least along the *b* axis in both co-crystals. The principal axes of the strain ellipsoid are not necessarily along the crystallographic axes in the monoclinic crystal system as the strain ellipsoid may be rotated about the monoclinic *b* axis. However, in **NOFN** and **AOFN**, the principal axes show the same trend as the crystallographic axes (Figures S4 and S5). The compression of the computed lattice parameters of the geometry-optimized **NOFN** and **AOFN** low-pressure structures is in excellent agreement with experiment. Computed unit cell axes are only slightly longer than experimental ones, which is a usual observation for such DFT calculations (Figures 4 and S6 and S7, Tables S11 and S12).[28] At the high-pressure phase transitions, the unit cells of **NOFN** and **AOFN** are severely distorted. The distortion mechanism is similar in both compounds, but much more severe in **NOFN** than in **AOFN**. The stacking axis (*a* axis) shortens by -18.8 % and -8.7 % in **NOFN** and **AOFN**, respectively, while the *c* axis increases by 6.6 % and 4.8 %, respectively, associated with a strong increase of the β angle (Figure 3). This may point to a rotation and/or slight slipping of the

molecules with respect to each other within the stacks. The strong shortening of the *a* cell parameter, which is the stacking direction of the molecules, at the phase transition indicates a discontinuous, strong reduction of the intermolecular separation distances. This points to a chemical reaction between the stacked molecules and the formation of new intermolecular σ-bonds (*vide infra*). Our observation for both **NOFN** and **AOFN** is consistent with the previously reported contraction of the *a* cell parameter in **NOFN** which was interpreted as being due to polymerization of the molecules along the stacks.[9]

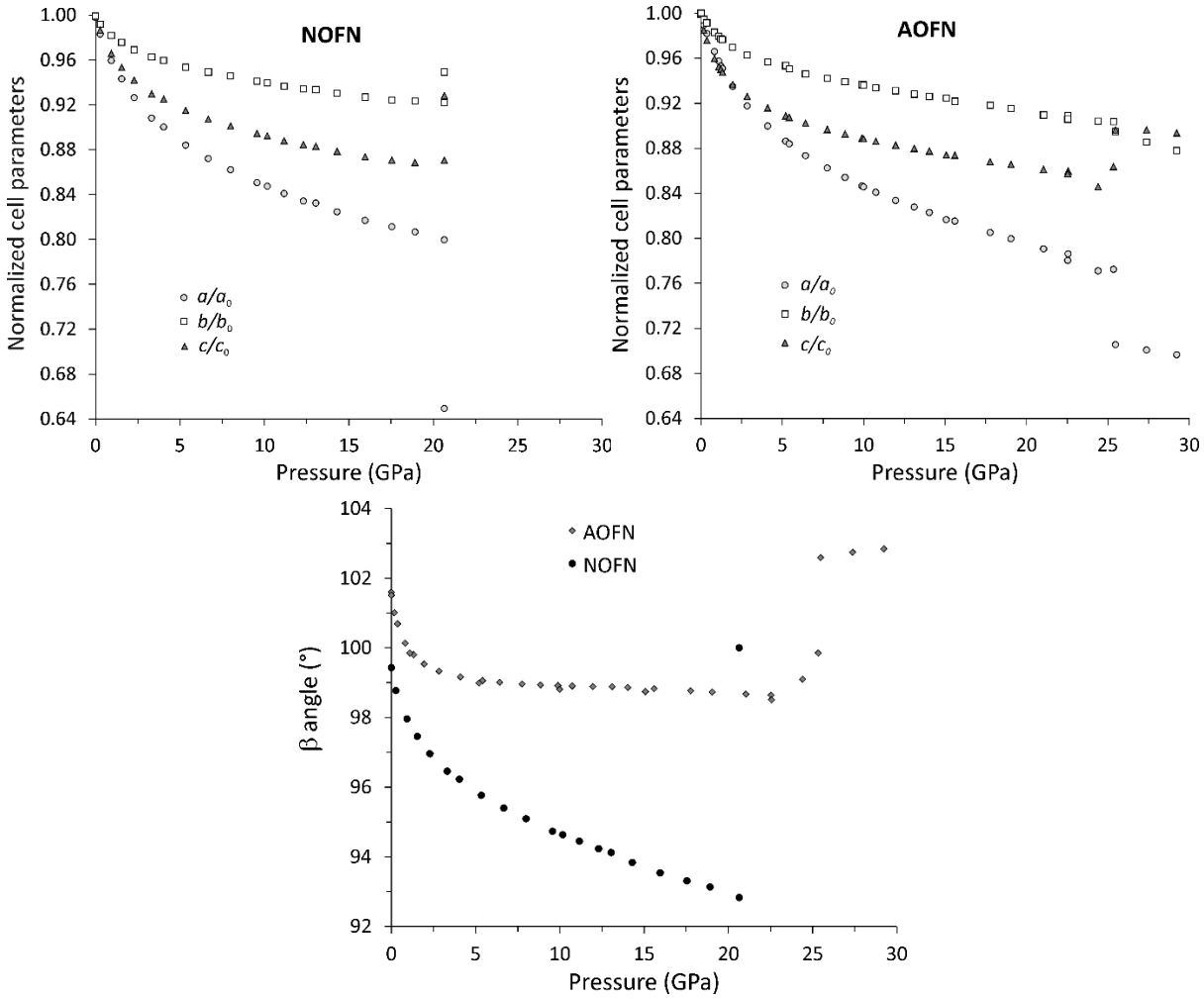

Figure 3. Pressure dependence of the normalized lattice parameters of **NOFN** (top left) and **AOFN** (top right), and of the monoclinic β angles of **NOFN** and **AOFN** (bottom). A pressure-induced phase transition or reaction is observed at ca. 20 GPa and 25 GPa in **NOFN** and **AOFN**, respectively. Note that in **NOFN** the unit cell parameters of both the low- and the high-pressure phase are plotted at 20.6(3) GPa. Only the data points from crystal 1 of **NOFN** are plotted, as the data from crystal 2 overlap with them within the symbol sizes.

In the earlier study on **NOFN**, the irreversibility of the pressure-induced phase transition was confirmed *via* diffraction during decompression and, hence, a polymerization process was proposed.[9] In order to check for a possible chemical reaction in the other co-crystal, **AOFN**, and to investigate the nature of the high-pressure phase transition, we performed two additional decompression studies on **AOFN**. In one run (run #2), a single crystal of **AOFN** was compressed to 25.6 GPa and wide scan images of broken single crystal parts of the high-pressure phase (Figure S3) were integrated as powder diffraction patterns and unit cell parameters were refined. Another crystal was compressed to 21 GPa (run #3) and single-crystal diffraction data were analyzed. However, the transition process was either not complete at 21 GPa or was slightly different due to the fact that the sample had been irradiated with a 40 mW 532 nm laser in an unsuccessful attempt to record Raman spectra. While the lattice parameters already indicated the distortion expected at the phase transition, i.e., the strong compression of the *a* axis (Figure 4), the unit cell volume did not show the strong reduction as in the runs at higher pressures due to a larger expansion of the *c* axis (Figure S7). We interpret this by a phase transition, which is concurrent with the onset of the chemical reaction, but was not complete at the lower pressure. Inspection of the decompression data clearly confirms that the phase transition is irreversible and that the high-pressure phase remains stable at ambient conditions (Figures 4 and S7). In particular, the irreversibility of the strong reduction of the crystallographic *a* axis, which is the π-stacking direction, upon decompression provides direct evidence of a chemical reaction, i.e., of pressure-induced polymerization (Figure 4).

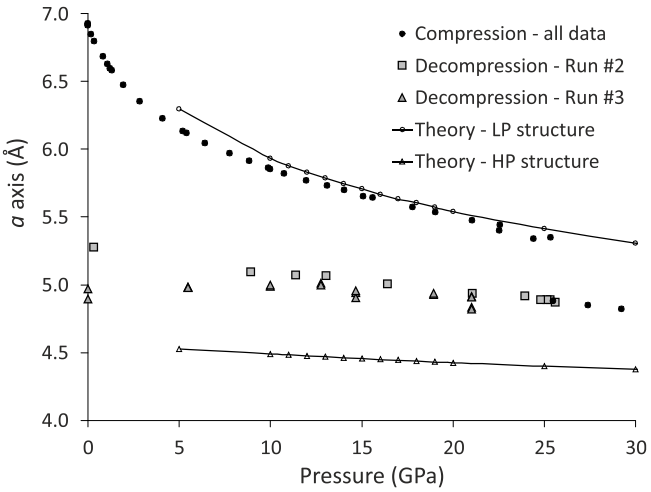

Figure 4. Evolution of the *a* cell parameter of **AOFN** on compression and decompression from experiment and theory (DFT). At about 25 GPa, a considerable shortening of the stacking direction is observed due to the pressure-induced phase transition. It is irreversible on decompression, suggesting a pressure-induced polymerization reaction. The data scatter on

decompression is larger than that of the compression data in the low-pressure phase, as only a few reflections of the high-pressure phase were observable up to a resolution of d = 1.2–1.5 Å. The solid lines are guides.

Both the rate of compression and pressure equilibration time, and perhaps laser irradiation, influence the onset pressure of the chemical reaction in **AOFN**. The onset of the phase transition was observed at a pressure of 24.4(1) GPa in the first experimental compression run, when the sample was equilibrated for ca. one hour between pressure steps. The crystal used in the second run remained in the low-pressure phase up to about 25.3(1) GPa upon faster compression, overshooting the reaction pressure, and transformed to the high-pressure phase on pressure equilibration overnight. In the third run, the pressure was increased to 21 GPa over a period of 9 days, during which the sample was irradiated with a laser (532 nm, ca. 40 mW) for several Raman measurements upon compression, and left at that pressure for 6 days before X-ray diffraction data were collected, which showed evidence of the unit cell deformation observed in the high-pressure phase. However, while the reaction may have been induced by the laser irradiation (i.e., a 2-photon absorption induced photopolymerization),[1a, 4k, 29] it was not complete at that lower pressure, as no significant reduction of the unit cell volume was observed.

Crystal structure analysis at high pressure

In order to understand the structural changes at the phase transition, it is crucial to have accurate structural data just before the transition. To the best of our knowledge, no crystal structures from single-crystal diffraction data have been reported on an aromatic compound up to a pressure close to the onset of polymerization.

The crystal structures of **NOFN** (space group $P2_1/c$) and **AOFN** (space group $P2_1/n$) were determined at ambient pressure at room temperature and at 100 K in order to serve as a reference for the high-pressure structures. Our structural parameters agree well with those reported for **NOFN** at room temperature[30] and for **AOFN** at 120 K[16d] (Tables S1 and S2). In both **NOFN** and **AOFN**, the centroids of all molecules lie on inversion centers of the unit cell (Figure 5). The stacks are related via the glide planes and the 2_1 screw axes are parallel to the b axis. Arene and octafluoronaphthalene molecules are alternately π-stacked along the a axis. Hence, the centroid-centroid distance between arene and octafluoronaphthalene molecules is equal to one half of the a cell parameter (Figures 1, 5 and S8).

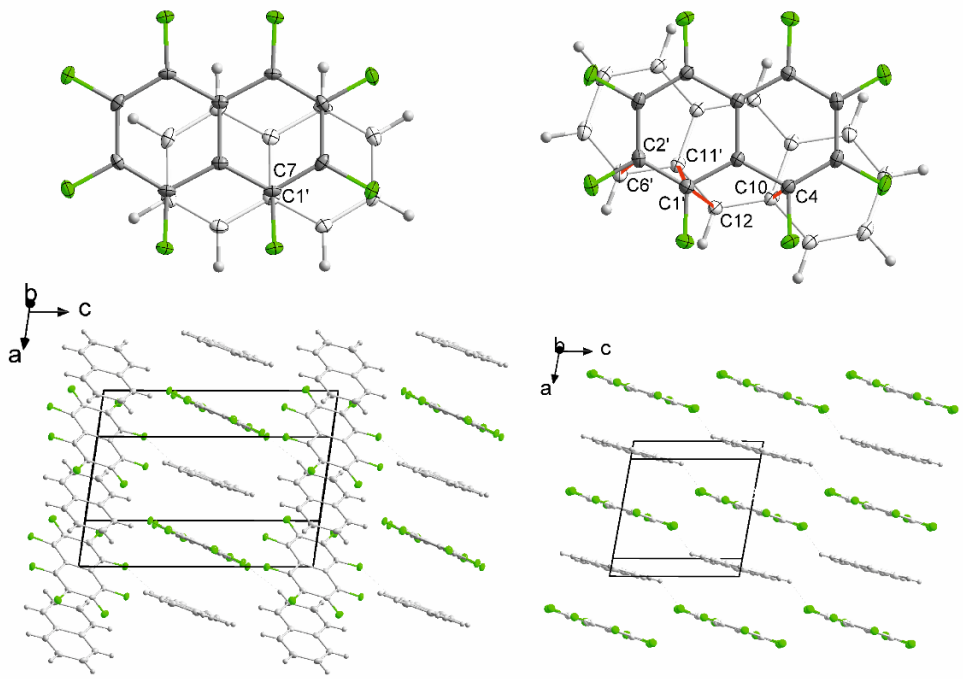

Figure 5. Top: Molecular overlap and π-stacking of octafluoronaphthalene (**OFN**) with naphthalene (left) and anthracene (right) viewed perpendicular to the **OFN** mean plane, at 100 K and ambient pressure. The centers of fluoroarene rings lie over C–C ring junction bonds of the arenes which is observed in many arene-perfluoroarene co-crystals.[16d, 19g] Nearest-neighbor intermolecular C···C distances (C7···C1' in **NOFN**, left, and C2'···C6', C1'···C11', C1'···C12, and C4···C10 in **AOFN**, right) are shown by red lines between labelled atoms. Bottom: Packing diagrams for **NOFN** and **AOFN**, showing the π-stacking of the components at 100 K and ambient pressure. Fluorine atoms are colored green in **OFN** molecules.

The main compression of the crystal structures of **AOFN** and **NOFN** is along the *a* axis, i.e., the π-stacking direction. This is directly associated with the strong compression of the inter-component centroid-centroid distance (= *a*/2, Figure 6) and, hence, the inter-component interplanar separations between the molecules which are π-stacked *via* the arene-perfluoroarene interaction (Figure 6). For **AOFN** especially, the compression of the *a* axis and, hence, of the centroid-centroid distances, closely corresponds to the compression of the intermolecular distances due to the small tilt of the molecules with respect to the *a* axis, which is represented by the small slip angles of 5.7° and 8.1° for anthracene and **OFN**, respectively (Figures 1, 5, 6, S8, and S9). In **NOFN**, the slip angles are larger, being 19.9° and 23.5° for naphthalene and **OFN**, respectively, hence the centroid-centroid distances are significantly longer than the interplanar separations (Figures 1, 6, S8, and S9). The mean inter-component interplanar distances of **AOFN** and **NOFN** are in the range of typical π–π stacking interactions;[31] in

NOFN, it is 3.47(5) Å, and is compressed by -19 % to 2.82(5) Å at the highest pressure of 18.9(1) GPa, whereas in **AOFN**, it is compressed by -22 % from 3.44(1) Å to 2.69(1) Å at 22.6(1) GPa (Figure 6, Tables S5 and S6). The DFT optimized structures of **NOFN** and **AOFN** between 1 and 25 GPa show very similar slip angles and only slightly larger distances compared to the experimentally determined ones, with stronger deviations for the distances at lower pressures of 1 – 5 GPa (Figures 6 and S9, Tables S18 and S19). The computed mean inter-component interplanar distances are compressed to 2.82 Å for **NOFN** at 20 GPa and to 2.68 Å for **AOFN** at 25 GPa. At higher pressures, a phase transition or chemical reaction takes place associated with a strong decrease of the *a* cell parameter by -8.7 % in **AOFN** (Figures 3 and 4). As the tilt angles of the molecules with respect to the *a* axis are very small in **AOFN**, a similar compression is inferred for the inter-component interplanar separation, which is extrapolated to be ca. 2.46 Å. This is below the critical nearest-neighbour (nn) intermolecular C···C distance of 2.6 Å at which the onset of polymerization reactions has been proposed from theoretical calculations.[1a] In **NOFN**, the compression of the *a* axis at the phase transition at 20.6(3) GPa is -18.8 %, more than twice of that in **AOFN**. If we consider the larger slip angles of the molecules in **NOFN**, and that they do not change at the phase transition, an extrapolation of the mean inter-component interplanar separation would result in a value of ca. 2.29 Å. However, if one considers the extreme case in which the slip angles drastically decrease to 0°, the maximum inter-component interplanar separation would become equal to the inter-component centroid-centroid distance and, hence, to half of the *a* axis, i.e., 2.43 Å at 20.6(3) GPa, a value close to that extrapolated for **AOFN** (2.46 Å) and again well below the critical nn (nearest-neighbor) C···C distance of 2.6 Å.

The pressure evolution of the nn C···C distances in **AOFN** and **NOFN** (labels and nn contacts are shown in Figure 5) show a similar trend (Figure 6, Tables S7 and S8). The shortest C1'···C7 distance in **NOFN** is compressed by -20 % from 3.384(13) Å to about 2.717(8) Å at 18.9(1) GPa (Table S7). The shortest C4···C10 and C2'···C6' distances in **AOFN**, which are both at the same sides of the molecules, are reduced by 23 and 22 % from 3.425(7) and 3.398(8) Å to 2.644(4) and 2.662(5) Å at 22.6(1) GPa, respectively (Figure 5, Table S8). Hence, the nn C···C distances before the phase transitions are close to the critical nn C···C distance of 2.6 Å proposed by Ciabini *et al.*[1a] Fitting 3rd-order Vinet[27] equations of state to the pressure dependence of the distances, and extrapolating those values to higher pressures, a distance of 2.70 Å is calculated for the C1'···C7 separation in **NOFN** at the phase transition pressure of 20.6 GPa, and of 2.63 Å for both C4···C10 and C2'···C6' separations at 25.4 GPa in **AOFN**. The values for the theoretically computed structures are ca. 2.71 Å for the C1'···C7 separation

in **NOFN** at 20 GPa and ca. 2.65 Å for both the C4···C10 and C2'···C6' separations in **AOFN** at 25 GPa (Figure 6, Tables S15 and S16). Again, while the compression behavior of the nn C···C distances of the computed **AOFN** structures is in excellent agreement with the experimentally determined ones, absolute values are slightly larger.

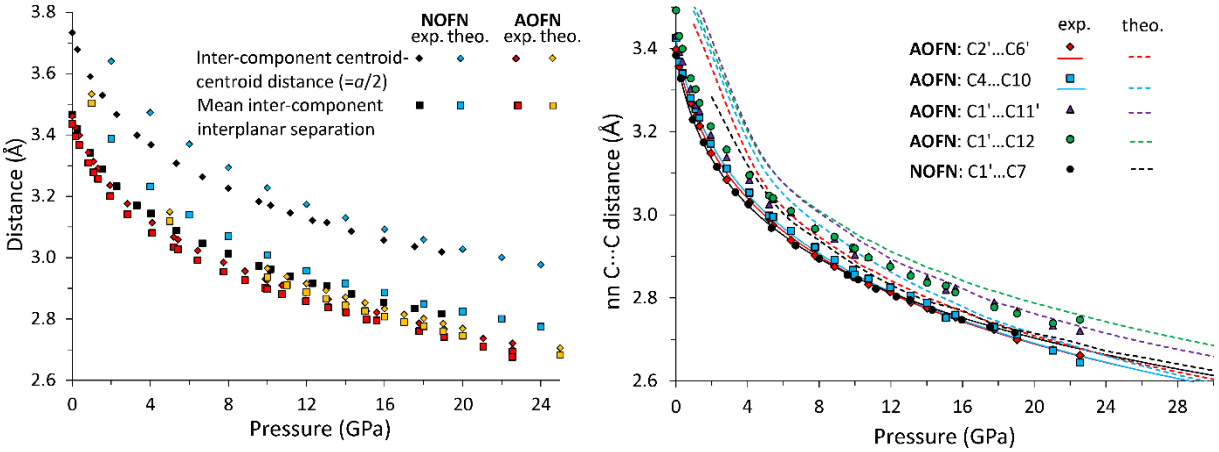

Figure 6. Pressure evolution of the (left) inter-component arene-**OFN** interplanar separations and centroid-centroid distances for **NOFN** and **AOFN** and (right) nearest-neighbor (nn) intermolecular C···C distances. Solid lines represent 3rd-order Vinet[27] equation of state fits to the pressure dependence of the nn C1'···C7 distance in **NOFN** and the C4···C10 and C2'···C6' distances in **AOFN**, while dashed lines represent computed data. See Figure 5 for the key nn C···C interactions in **NOFN** and **AOFN**.

As the nn C···C distances are arranged nearly parallel to the stacking axes, we conclude that they decrease well below 2.6 Å at the phase transition. This supports the interpretation of the phase transition being associated with a polymerization reaction. Interestingly, the orientations of the molecules relative to one another, and the slip angles of the arene and **OFN** molecules, vary within only 1–2° on compression up to the highest pressures obtained before the phase transitions (Figure S9, Tables S5 and S6). Hence, the interstack H···F contacts,[16d, 19a, 19k] which are present *between* the columns of both **NOFN** and **AOFN** structures decrease upon compression only as a result of the free volume reduction between the molecules. In agreement with previous results on **NOFN**,[9] our results show that the arene-perfluoroarene interaction leads to a very stable molecular arrangement in both **NOFN** and **AOFN** up to very high pressures, shortly before chemical reaction and loss of aromaticity takes place. The strengthening of intermolecular interactions at high pressure can be visualized *via* Hirshfeld surface plots[32] of the low-pressure structures of **NOFN** and **AOFN** at ambient and highest pressures which reveal an increase in the C···C and C···F intermolecular close-contact fractions and a decrease in the H···F ones (Figures S12 and S14 in the S.I.).

The intramolecular C–C and C–F bonds are only slightly shortened (0.02 Å on average) over the whole pressure range studied (Figures S15-S20, Tables S7 and S8). This total compression is within 2–4 standard uncertainties (s.u.) of the bond lengths, considering the actual errors from the scatter of the pressure evolution of the C–C and C–F bond distances (Figures S15-S20). The actual errors are estimated to be in the range of ±0.013 Å for the data sets of one single crystal and ±0.005 Å for the combined data sets from two **NOFN** crystals, and are slightly larger than the s.u.'s obtained from the structure refinements (Tables S7 and S8). Bond distances at ambient conditions are least reliable due to the strong thermal atomic motions. The C–C and C–F compression of the computed **NOFN** and **AOFN** structures is in the same range as the scatter of the experimental data (Figures S15-S20, Tables S15 and S16). Our data confirm that the C–C distances are still in the range of aromatic bonds at the highest pressures of single-crystal structure refinements at 18.9(1) GPa for **NOFN** and at 22.6(1) GPa for **AOFN**. Nevertheless, the onset of the phase transition is observed in the crystal structure of **NOFN** at 18.9(1) GPa by a strong increase of the displacement parameters which reflects an increased uncertainty of the atom positions and hence a decrease of the quality of the two single crystals (Figure 7). The loading of two **NOFN** crystals of different orientations, and combined refinement of the intensity data, increased the data:parameter ratio and, hence, enabled the stable refinement of reliable anisotropic displacement parameters (U_{ij}), which are all positive without applying restraints in the structure refinements (Table S9). In Figure 7, the pressure evolution of the mean equivalent displacement parameters of atom groups with similar bonding environment and, hence, vibrations is shown. In general, pressure increase leads to a decrease of atomic thermal motions as is observed upon temperature decrease. The effect is especially strong for molecular organic crystals.[33] If we compare the displacement parameters of **NOFN** at 100 K with the high-pressure trend, the motions would correspond to those of **NOFN** at a pressure between 5 and 6 GPa. In comparison, the atomic motion of *syn*-1,6:8,13-biscarbonyl[14]annulene studied at 7.7 GPa by Casati *et al.* was found to correspond to the thermal motions of this compound at 123 K.[33] At the highest pressure, the unusual increase of the displacement parameters indicates the onset of the reaction. To the best of our knowledge, a similar accurate evolution of the decreasing anisotropic displacement parameters of an aromatic molecular compound, in our study up to 18 GPa, has not been previously reported at pressures > 10 GPa.

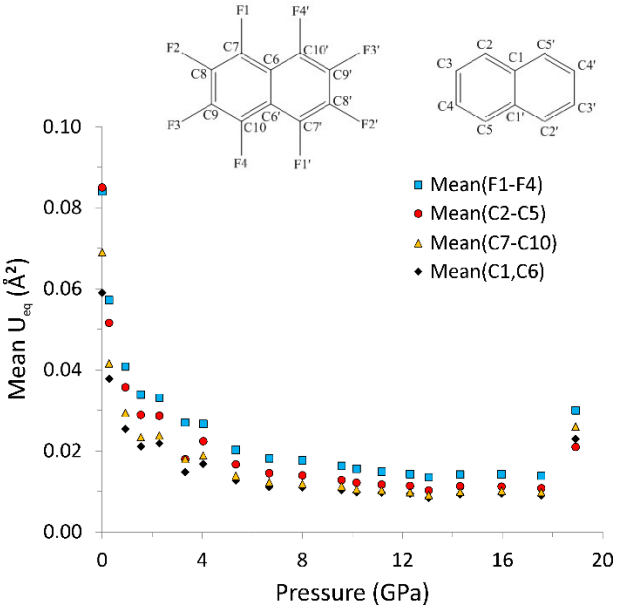

Figure 7. Pressure dependence of the mean equivalent displacement parameters U_{eq} (Å²) from the combined refinement of the **NOFN** data sets. At 3.32(1) GPa, only a single data set from one crystal was refined. At 18.9(1) GPa, the quality of both crystals decreased resulting in reflection broadening, a lower data:parameter ratio and, hence, larger displacement parameters.

Crystal structures of the polymerized columnar hydrofluorocarbons from theoretical computations

On geometry optimization of the low-pressure crystal structure of **NOFN** in space group $P1$ at 20 GPa, a fully polymerized structure for the high-pressure phase was obtained computationally, for which unit cell parameters are in excellent agreement with our experimental data from single-crystal X-ray diffraction (Tables 1 and S3). While computed unit cell angles of the polymer structure point to a monoclinic symmetry, the structure slightly deviates from monoclinic ($P2_1/c$) symmetry and resembles triclinic symmetry (space group $P1$). We kept the unit cell setting and atomic parameters comparable to the low-pressure phase ($P2_1/c$ setting) for better comparison (β = 106.5°). Another setting corresponding to the pseudo-monoclinic $P2_1/n$ symmetry (β = 96.5°) would be the standard setting (Table S3). The geometry of the crystal structure of **AOFN** was optimized in space group $P1$, taking the low-pressure structure determined at 18.9(1) GPa as the starting geometry, at a much higher pressures of 50 and 120 GPa than reached in our experiments, and fully polymerized high-pressure structures were obtained, showing similar structural features. Indeed, both computed structures had $P2_1/n$ space group symmetry, and, after re-optimization at different pressures, we found that both resemble the same polymer structure. The unit-cell parameters of the computed high-pressure

structure ($P2_1/n$) agree well with our experimental data at ca. 30 GPa (Tables 1 and S4). Data of the computed crystal structures are given in the Supporting Information (Tables S13 – S14). The stable phases at these pressure conditions are fully polymerized along the arene-perfluoroarene π-stacking direction (Figures 8, S32, and S33). They form broad columns of σ-bonded sp^3 carbons with the breadth of the columns depending on the extension of the polycyclic arenes involved, i.e., **AOFN** forming laterally more extended columns than **NOFN**. However, at the outer edges of the anthracene unit, two pairs of doubly-bonded sp^2 carbons remain, with C–C bond lengths of 1.305 Å at 30 GPa (Figure 9). All bond distances of the polymerized phases are illustrated in Figure 9. In **NOFN**, Csp^3–Csp^3 bond lengths at 20 GPa are 1.488–1.553 Å in the naphthalene unit, 1.478–1.548 Å in the octafluoronaphthalene unit, and 1.470–1.619 Å for the σ-bonds connecting the units. In **AOFN**, Csp^3–Csp^3 bond lengths at 30 GPa are 1.480–1.521 Å in the anthracene unit (Csp^3–Csp^2 = 1.455–1.484 Å, Csp^2–Csp^2 = 1.305 Å), 1.504–1.552 Å in the octafluoronaphthalene unit, and 1.493–1.538 Å for the σ-bonds connecting the units. Hence, bond lengths of the **AOFN** polymer vary within a smaller range than those of the **NOFN** polymer.

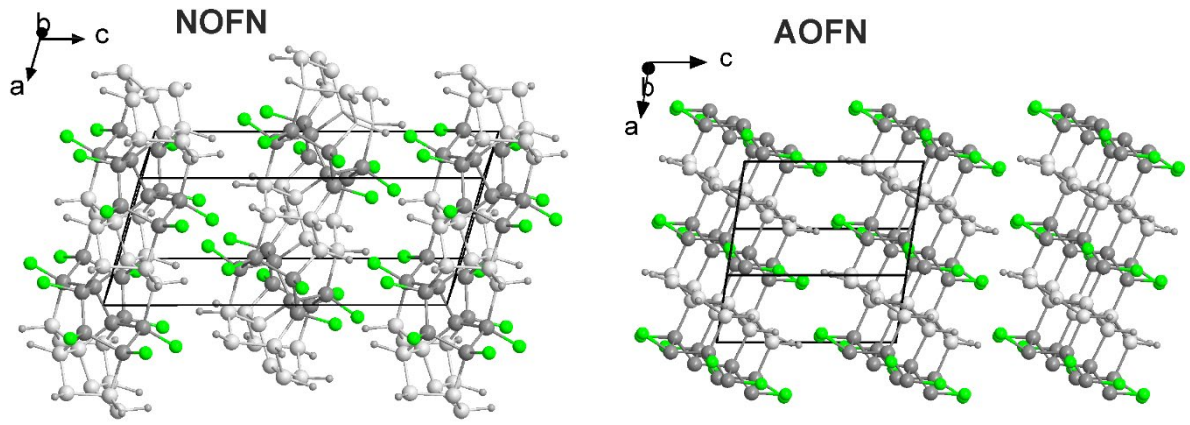

Figure 8. Crystal structures of the fully polymerized high-pressure phases of **NOFN** at 20 GPa (left) and **AOFN** at 30 GPa (right) as obtained from theoretical calculations. Columns of hydrofluorocarbons are formed along the *a* axis.

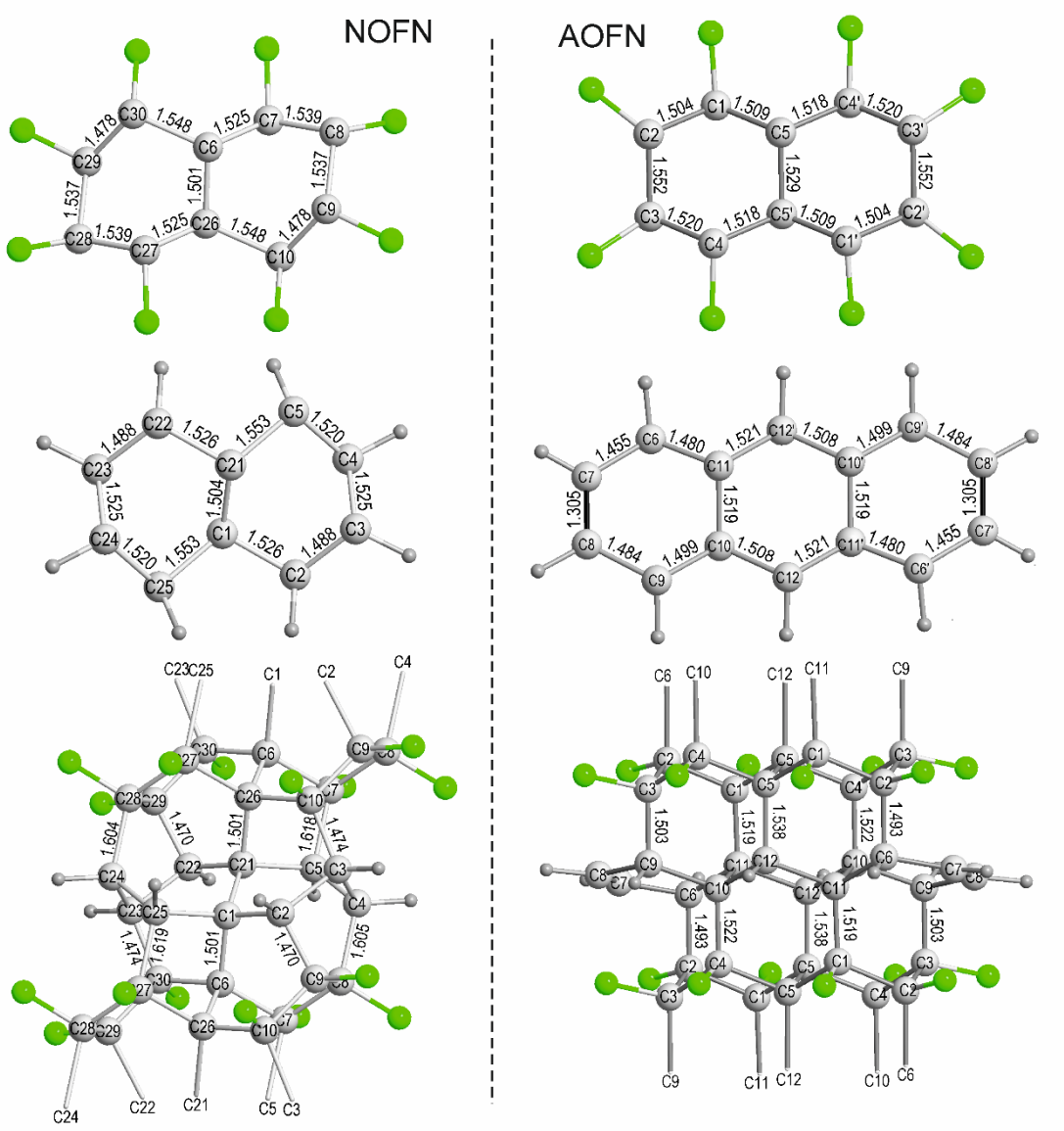

Figure 9. C–C bond distances (Å) of the polymerized **NOFN** (left) and **AOFN** (right) high-pressure phases in the octafluoronaphthalene unit (top), naphthalene or anthracene unit (middle), and between the fluorocarbon and hydrocarbon components (bottom) in the column of σ-bonded sp^3 carbons at 20 and 30 GPa, respectively. The C–C double bonds in the anthracene unit are drawn in black (middle). For **NOFN**, distances are shown for only one of two similar, but symmetry-independent columns.

The computed structures of the **NOFN** and **AOFN** polymers are very different as a result of the different number of benzene rings in the naphthalene and anthracene molecules. In the **NOFN** polymer, the 6-membered rings of the naphthalene and octafluoronaphthalene units have twist boat conformations with a pseudo-inversion relation within each unit. The units are interconnected via 5-, 6-, and 7-membered carbon rings, of which the 6-membered rings have boat conformations (Figure 10). The columns extending along the *a* axis can be considered as

double threads, the single threads related to each other via pseudo-inversion symmetry. Considering only the bonding of the carbon atoms and neglecting the hydrogen and fluorine substituents, a single thread resembles the conformation of a zipper polymer as reported by Chen et al. for one possible benzene nanothread conformation.[4o, 6b] Hence, the **NOFN** polymer can best be described as an H-F-substituted double-thread zipper polymer. Based on this, we propose a reaction mechanism starting with Diels-Alder [4+2] cycloaddition reactions followed by zipper reactions on both benzene rings of the naphthalene units (Figure 10). A similar reaction mechanism was recently proposed for **NOFN**.[9] Although the authors have reported two computed structural models for the **NOFN** polymer phase, they did not provide any structural data, i.e., no unit cell parameters, atomic coordinates, or bond lengths were presented.[9] Hence, we cannot compare our experimental unit cell data nor our computed model with their simulated models. However, our model agrees better with the [4+2] cycloaddition model than with the 2A-tube model.[9] In contrast to **NOFN**, in **AOFN** the number of benzene rings in anthracene and **OFN** molecules differ by one. This prevents the formation of a tube-like polymer arrangement. Instead, C–C bond formation between the molecules is favorable in a diamondoid-type way[34] forming columns of face-sharing diamantanes along the stacking axis. Hence, the rings of the anthracene units are shifted with respect to those of the **OFN** molecules by half a ring when viewed down the stacking axis, with the double bonds remaining at both ends of the anthracene units (Figure 10). We propose a straight zipping reaction between the anthracene and **OFN** molecules resulting in a diamondoid polymer as illustrated in Figure 10. Similar to the crystal structure of diamond, all carbon rings are 6-membered, including the interconnecting rings, and have chair conformations.

The columnar arrangement of the polymer structures for the **NOFN** and **AOFN** high-pressure phases is different than the arrangement of the nanothread tubes proposed previously for polymerized aniline and pyridine.[7a, 7b] In contrast to most other studies on PIP of aromatic compounds, except that of Ward *et al.*,[9] in the cases of **NOFN** and **AOFN**, the reaction involves polycyclic aromatic hydrocarbons and fluorocarbons, hence resulting in broader columns, when compared to benzene, aniline or pyridine nanothreads (Figures 8 – 10, S32 and S33).

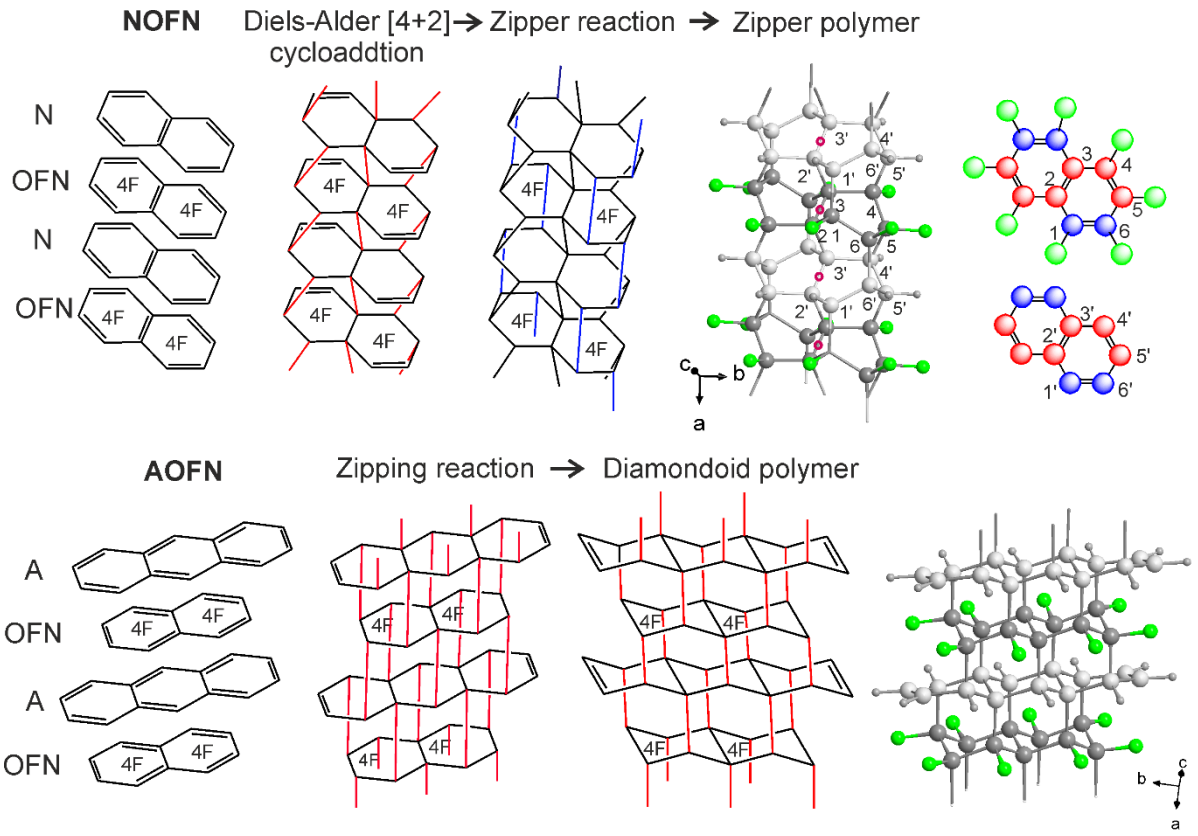

Figure 10. Sketches of the potential reaction pathways of the naphthalene (**N**) / anthracene (**A**) and octafluoronaphthalene (**OFN**) molecules along the stacking direction. In **NOFN** (top), a Diels-Alder [4+2] cycloaddition reaction (red lines indicate C–C bond formation) followed by a Zipper reaction (blue lines represent C–C bond formation) is proposed in order to form a fully saturated carbon double thread. In the columnar Zipper polymer, red circles represent pseudo-inversion centers relating the single threads to one another. Carbon atoms are numbered according to the schemes of the **OFN** and **N** molecules on the right. Red and blue atoms indicate carbon atoms involved in the [4+2] reaction and the Zipper reaction, respectively; green: fluorine, grey: hydrogen. Interconnecting carbon rings between the **N** and **OFN** units are 5-membered (-6-6'-5'-4'-5- and -1-2-3-2'-1'-), 6-membered (-2-3'-4'-5-4-3- and -2'-3-4-5'-4'-3'-), and 7-membered (-1-2-3'-2'-1'-6'-6- and -1'-1-6-5-4-5'-6'-). In **AOFN** (bottom), a straight zipping reaction between the inner carbon atoms of one unit and the outer carbon atoms of the other unit is proposed, leading to a diamondoid polymer structure. Note the remaining double bonds at both ends of the anthracene units.

While overshooting the experimental pressure of the reaction was necessary and expected in the theoretical calculations of **AOFN** in order to obtain a polymerized structure, the pressure evolution of the total energy per unit cell for both the low- and the high-pressure structure shows that the polymerized phase is already the stable phase at pressures above 11 GPa (Figure S34).

This is a much lower pressure than the experimentally observed reaction pressure (ca. 25 GPa). However, the energy differences are thermodynamic quantities and thus do not take into account transition state kinetic barriers or very slow dynamic processes, which are observed in both the X-ray diffraction and IR spectroscopic experiments. They show the influence of equilibration time on the onset pressure of the reaction, and the slow kinetics of the polymerization reaction.

The pressure dependence of the unit-cell parameters of the computed low- and high-pressure structures of **AOFN** are shown in Figures 4 and S7, and are listed in Table S12. As the computed *a* lattice parameter and β angle of the **AOFN** high-pressure phase are smaller while the *b* lattice parameter is slightly larger than the experimental values, further computations were performed to stabilize a dimer or different polymer by alternatively increasing and decreasing gaps between molecular pairs, sliding one molecule over another, or rotating one of the molecules a little bit. However, these calculations have always resulted in either a molecular or a fully polymerized structure. Nevertheless, the longer experimental *a* axis, which is the π-stacking direction, if compared to the computed one, could be an indication of a metastable dimerization or only partial oligomerization of the high-pressure structure of **AOFN** due to the high kinetic energy barrier in the experiment.

Kinetics of the polymerization reaction from high-pressure infrared spectroscopy

The occurrence of a polymerization reaction instead of a simple phase transition was additionally confirmed by high-pressure IR spectroscopy on both **NOFN** and **AOFN**. Samples were pressurized several times in different pressure media (see Supporting Information for more details) until the onset of the reaction was observed, and the time evolution of the IR absorption spectra and, hence, of the reaction was investigated at that pressure. The influence of successive pressure increase on the reaction was studied for **AOFN** as well. The mid-IR spectra can, in general, be interpreted as a combination of IR modes from each of the molecules of the co-crystals, i.e., of naphthalene and **OFN** modes for **NOFN**, and of anthracene and **OFN** modes for **AOFN**. Typical overall assignment of the IR modes in hydrogenated aromatic systems at ambient conditions is grouped as follows: C–H stretching bands in the 3100 – 3000 cm^{-1} range, C=C stretching bands at 1620 – 1430 cm^{-1}, in-plane ring deformation vibrations bands at 1300 – 1000 cm^{-1}, and out-of-plane C–H bending vibrations at 910 – 660 cm^{-1}.[35] C–F stretching and C–F deformation bands appear in the 1270 – 1100 cm^{-1} and 910 – 660 cm^{-1} regions, respectively, in perfluorinated aromatic systems. In single-bonded hydrocarbons as expected for the polymers, the sp^3 C–C stretching and C–H bending vibrations are usually in the 1250 –

910 cm^{-1} region at ambient conditions. Upon pressure increase, the mode frequencies, in general, show a blue shift due to the increasing bond strength, as is also observed for most of the IR modes of **NOFN** and **AOFN** (Figures S27 – S28 and S30 – S31, respectively, in the Supporting Information). Soft-mode behavior is detected for two IR modes at 666 cm^{-1} (at 0.77 GPa; 654 cm^{-1} at 20.3 GPa) and 679 cm^{-1} (at 4.22 GPa; 672 cm^{-1} at 20.3 GPa) in **NOFN**, and for two weak IR modes between ca. 650 and 700 cm^{-1} (635.5 and 664 cm^{-1} at 21 GPa), a mode at 1270 cm^{-1} and two modes between ca. 1390 – 1410 cm^{-1} for **AOFN**. The soft modes between 600 and 700 cm^{-1} (at the pressure of polymerization) are assigned to out-of-plane ring deformations of the carbon skeletons of the **OFN** and naphthalene molecules in the co-crystals (Figures S37 and S38). As these out-of-plane deformations are in the directions of the stacking axis and, hence, of the intermolecular bond formation, a relationship between these soft modes and the intermolecular bonding process at polymerization may exist. However, to prove this, an extensive computational study would be required which is beyond the scope of our study. At close to 15 GPa, a new mode appears at 644 cm^{-1} in **NOFN**, while the appearance and increase of intensity of a new mode at 1147 cm^{-1} is already observed at 12 GPa (Figures S26 and S28). This mode arises as a shoulder of another strong mode at slightly higher frequency, which decreases in intensity as a consequence of the increase of the new mode.

In spite of the appearance of the subtle modes just mentioned, the overall features of the spectrum do not show relevant changes up to the onset of reaction at 17 – 20 GPa for **NOFN**, while for **AOFN** it was observed at a higher pressure of ca. 22 GPa in KBr and argon pressure-transmitting media (PTM), and at ca. 24–25 GPa in more hydrostatically behaving liquid nitrogen and helium PTM. The intensities of the strong IR modes of both **NOFN** and **AOFN** pristine co-crystals decrease with reaction time and with pressure, while an increase in the background signal is present in the 1000 – 1450 cm^{-1} region (Figures 11 – 12, and S21 – S25 in the Supporting Information). This is consistent with the formation of sp^3 carbon atoms. As stated above, sp^3 C–C and C–F stretching modes as well as sp^3 C–H bending and C–C deformation modes of the polymer are expected in this range. In the 1450 – 1800 cm^{-1} range, all modes decrease in intensity and, as those modes are typically due to sp^2 C=C stretching vibrations, this is a clear evidence for the polymerization reaction, bond formation, and, hence, loss of aromaticity. Our observation for **NOFN** is in agreement with the IR analysis of the recent reaction study on **NOFN** by Ward *et al.*[9]

We computed the phonons of both the low- and high-pressure phases of **NOFN** and **AOFN** at the reaction pressure using a density functional perturbation theory (DFPT) method[36] (Figures

13 and 14, Tables S20 and S21 in the S.I.). Theoretical results are in excellent agreement with the experimental observations. Compared to the strong IR modes of the **NOFN** and **AOFN** low-pressure structures, the respective computed modes are systematically red-shifted by 20 – 40 cm^{-1} (Table 2, Figures S35 and S36, Tables S20 and S21 in the Supporting Information).

Table 2. Comparison of the strongest IR modes (cm^{-1}) of the NOFN and AOFN co-crystals and polymers from experiment (exp.) and theory (theo.).

NOFN			**AOFN**		
Co-crystal, exp., 21 GPa	Co-crystal, theo., 20 GPa	Polymer, theo., 20 GPa	Co-crystal, exp., 25 GPa	Co-crystal, theo., 25 GPa	Polymer, theo., 25 GPa
821	803	1082	761	746	855
1002	972	1106	990	985	955
1480	1446	1118	1000	991	975
1557	1521	1147	1270	1233	1052
1745	1712	1176, 1182	1484	1423, 1433	1220, 1224
		1250	1514	1488, 1496, 1503	1247
		1308, 1317	1561	1522, 1530	1399
		1336	1746	1704	

The IR modes of the calculated polymerized high-pressure structures have weak to moderate intensities compared to those of the low-pressure structures, with an accumulation of significantly intense bands between ca. 1050 and 1350 cm^{-1} for **NOFN** at 20 GPa and ca. 955 and 1400 cm^{-1} for **AOFN** at 25 GPa, respectively. The strongest bands in the IR spectrum of the calculated polymerized **NOFN** phase are accumulated in the 1080 – 1180 cm^{-1} and 1300 – 1380 cm^{-1} regimes (Figure 13). The bands at 1082 and 1106 cm^{-1} correspond to sp^3 C–C deformation, while the bands at 1118, 1176 and 1182 cm^{-1} are due to a combination of C–C–H bending with C–C and C–F stretching vibrations of the polymer. Similarly, the strongest calculated bands of the polymerized **AOFN** phase are at 955 cm^{-1} (sp^3 C–C deformation), and at 1220 and 1224 cm^{-1} (C–H deformation) (Figure 14). They are consistent with the increase of the background signal in this spectral range observed in both, **NOFN** and **AOFN**, on reaction progress. In particular, for the chemical reaction of **AOFN** in argon PTM, which proceeded very slowly at 22 GPa, a slight intensity increase with time is only observed at ca. 900, 1050, 1200 – 1250, and 1400 cm^{-1} (Figure 12). These spectral regions are fully consistent with those

of the strongest calculated modes of the **AOFN** polymer (Table 2), and, hence, this is consistent with the formation of the polymer structure.

While strong IR modes are present in the 1450 – 1750 cm^{-1} region in **NOFN** and **AOFN** co-crystals at 20 and 25 GPa, respectively, no IR modes are predicted for the **NOFN** polymer in this region, and only a few extremely weak modes of unobservable intensity are predicted for the **AOFN** polymer (Figures 13 and 14). This is consistent with the observed decrease of the strong modes in this spectral region on reaction progress and with the absence of strong sp^2 C=C stretching vibrations in the polymer structures. For example, the IR mode observed in **NOFN** at 1745 cm^{-1} (at 20 GPa) is an sp^2 C=C stretching band of the aromatic **OFN** molecule and should no longer be present in the polymer. Hence, it was used for the determination of the amount of reacted monomer (see below). Note that in **AOFN** not all of the aromatic C–C bonds become Csp^3–Csp^3 single bonds upon polymerization, and also that Csp^3 – Csp^2 bonds and sp^2 C=C double bonds are formed in the polymer due to the mismatch of the anthracene and **OFN** molecules. Thus, sp^2 C=C double bonds remain at the outer edges of the anthracene molecules, which explains the theoretical prediction of some weak modes in this spectral region.

Theoretical calculations do not predict any vibrational modes between 1800 cm^{-1} and 3000 cm^{-1} for any of the phases investigated. At 1800 – 2600 cm^{-1}, the strong IR absorbance of the diamond anvils of the pressure cell is dominant in our experiments. ν_{C-H} stretching modes are predicted at ca. 3200 – 3300 cm^{-1} in the **NOFN** co-crystal structure at 20 GPa and at ca. 3150 – 3250 cm^{-1} in the polymerized structure at 20 GPa (Figure 13). These modes occur at slightly higher energies for the **AOFN** co-crystal (3250 – 3400 cm^{-1} at 25 GPa) and span a wider range for the **AOFN** polymer (3050 – 3470 cm^{-1} at 25 GPa). The ν_{C-H} stretching modes are weak and not well resolved in our experiments so that only the decrease of IR absorbance is observed with time in this region (Figure 11 and S24 in the Supporting Information). For the ν_{C-H} stretching modes of both naphthalene and anthracene, it was previously reported that the theoretically calculated absorption intensities are consistently overestimated by a factor of ca. 2 when compared with experimental intensities.[37] Such an overestimation is also observed in our study on the arene-perfluoroarene co-crystals.

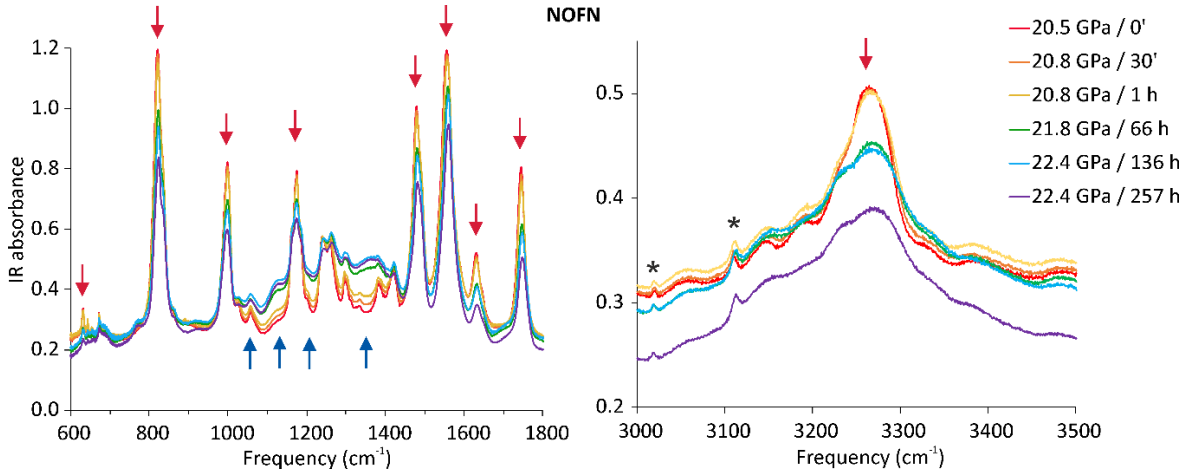

Figure 11. Infrared absorption spectra of **NOFN** in KBr pressure medium at pressures ranging from 20.5 to 22.4 GPa in the spectral range from 600 to 1800 cm^{-1} (left) and from 3000 to 3500 cm^{-1} (right). After reaching 20.5 GPa, significant changes of the intensities are observed as a function of time indicating the progress of a chemical reaction. Red arrows designate the decrease in IR mode intensities while blue arrows designate the increase in IR absorbance with time. Asterisks indicate IR modes that do not belong to **NOFN**. Their sharpness suggests that they are due to impurities outside the pressure chamber of the diamond anvil cell.

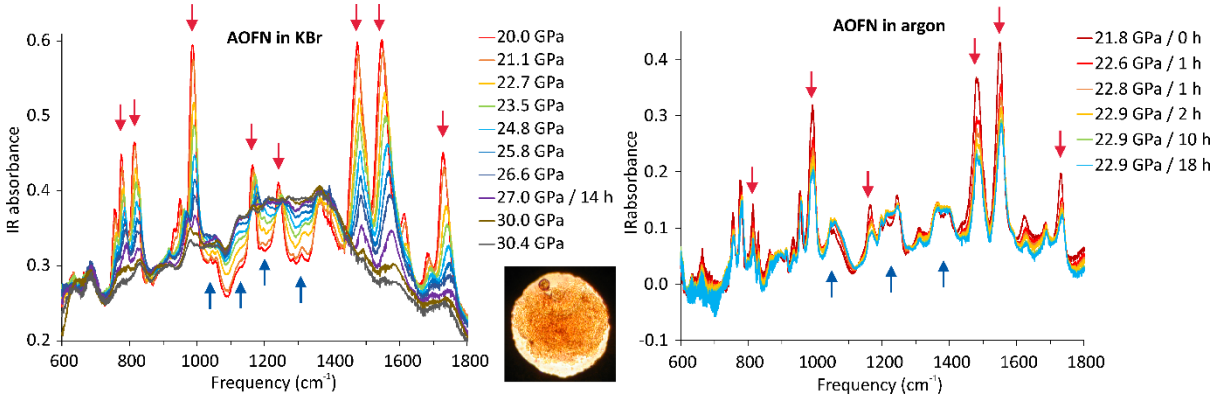

Figure 12. Infrared absorption spectra of **AOFN** during its chemical reaction upon pressure increase from 20.0 to 30.4 GPa in KBr pressure medium (left) and at ca. 22 GPa as a function of time in an argon pressure medium (right), both in the spectral range from 600 to 1800 cm^{-1}. Significant changes of the intensities are observed upon increasing pressure and with time indicating the progress of a chemical reaction. Red arrows designate the decrease of the strongest IR mode intensities while blue arrows designate the increase of IR absorbance with time. The picture in the bottom center shows the reacted sample disc – the sample became orange colored upon polymerization – and a ruby ball in the KBr pressure medium, after pressure quenching at ambient pressure before opening the diamond anvil cell. The diameter of the sample chamber is ca. 150 µm.

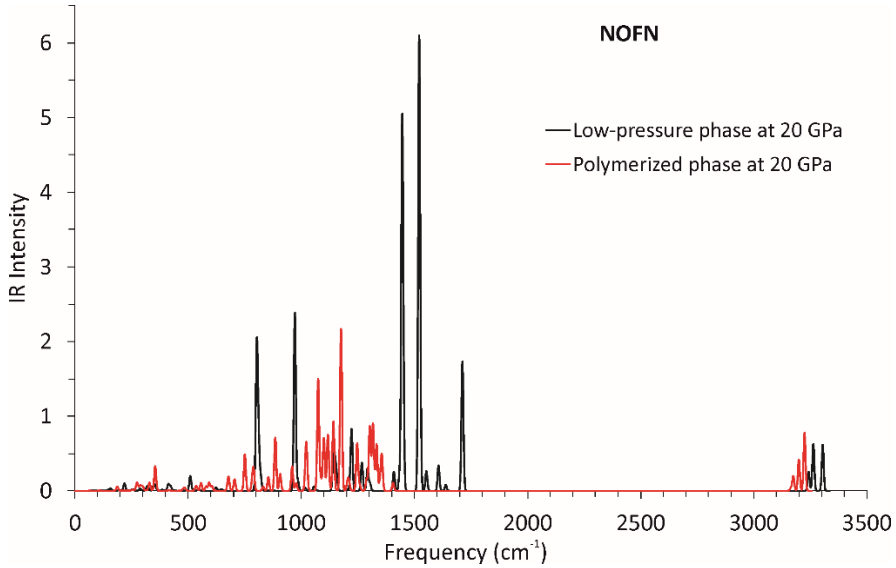

Figure 13. Computed infrared absorption spectra of the **NOFN** molecular structure (black line) and the **NOFN** polymer structure (red line) at 20 GPa. Note the lower IR mode intensities of the polymer structure.

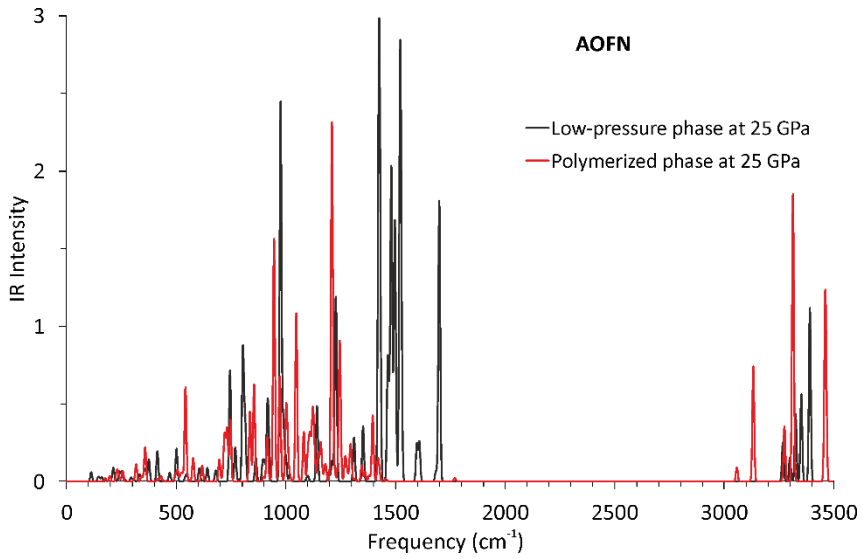

Figure 14. Computed infrared absorption spectra of the **AOFN** molecular structure (black line) and polymer structure (red line) at 25 GPa.

The amount of reacted sample was determined from the decrease of the integrated areas of the IR absorbance bands at 1745 cm^{-1} at 20.5 GPa for **NOFN**, at 820 cm^{-1} at 25.5 GPa for **AOFN** in a nitrogen PTM, and, due to broader modes and more severe overlap of IR modes, at 1550 cm^{-1} at 22 GPa for **AOFN** in a less hydrostatic argon PTM (Figure 15). From this we can determine the amount of unreacted sample during the reaction. The data were analyzed with a

modified Avrami model.[38] The fitting equation is $R_t = R_\infty \cdot (1 - e^{-k(t-t_0)^n})$, where $R_t = 100 \cdot (\frac{A_0 - A_t}{A_0})$ is the reacted reagent ratio with A_0 the absorbance of a reagent band at initial time and A_t the absorbance of the same band at a subsequent time *t*. R_∞ is the reaction yield at the end of the reaction, $k^{1/n}$ is the reaction rate, and *n* is a parameter depending on the topochemistry of the process and increases with the dimensionality of the process (Figure 15). Originally, the Avrami model was developed to describe the kinetics of crystal growth from a liquid phase.[39] When only the growth step is taken into account, the *n* values of 1–2, 2–3, and > 3 indicate linear, two- and three-dimensional growth processes, respectively. However, if the nucleation process is considered, as in our case, the *n* values change according to the nucleation rate and the mechanism controlling the nucleation step.[40] For $n < 1$, linear growth is unambiguous. The fit of the data to the Avrami model results in $n = 0.36$ (run in a KBr PTM) and $n = 0.38$ (run without a PTM) for **NOFN**, and in $n = 0.58$ (run in a nitrogen PTM) for **AOFN** (Figure 15). For the kinetic data of **AOFN** in argon, we can only estimate the values because, after ca. 24 h, further significant progress of the reaction was observed as a result of laser irradiation of the sample. The laser with a wavelength of 532 nm (ca. 1 mW power on the sample) was used in order to induce the fluorescence of a small ruby ball within the pressure chamber, the shift of which is used for pressure determination.[41] With $n = 0.45$ and $k^{1/n} = 0.45$, we can reproduce both the rapid rate at the beginning of the reaction followed by the slow rate on a long time scale (> 24 hours) (Figure 15). A similar effect of laser light on the reaction was observed in **NOFN** (*vide infra*) (Figure S21). All of the values for *n* are close to 0.5, a value which was correlated to a one-dimensional, diffusion-controlled growth process.[40] This confirms our proposed mechanism of polymerization along the columns of π-stacked arenes and perfluoroarenes in both **NOFN** and **AOFN**. Our study shows that the reaction is very slow at ambient temperature. After 24 hours, between 20 and 26 % of the **NOFN** and **AOFN** sample have reacted; however, after 6 days, the reacted portion is only < 30 %. The reaction yield is between ca. 30 and 40 % for **NOFN** and **AOFN** at constant pressure and temperature. The low yield is consistent with a reaction driven by the uniaxial stress due to the compression direction. It was discussed previously, with respect to pressure-induced nanothread formation in pyridine, that only the portions of the sample aligned with the stress direction react to give threads.[7c] None of the pressure media used in our IR studies provides hydrostatic conditions at the polymerization pressures,[26, 42] nor are the samples soft at these pressures, as is evident from their equations of state (Figure 2). Hence, non-hydrostatic stress is clearly present in these samples and needs to be considered in the selection of the reaction path.

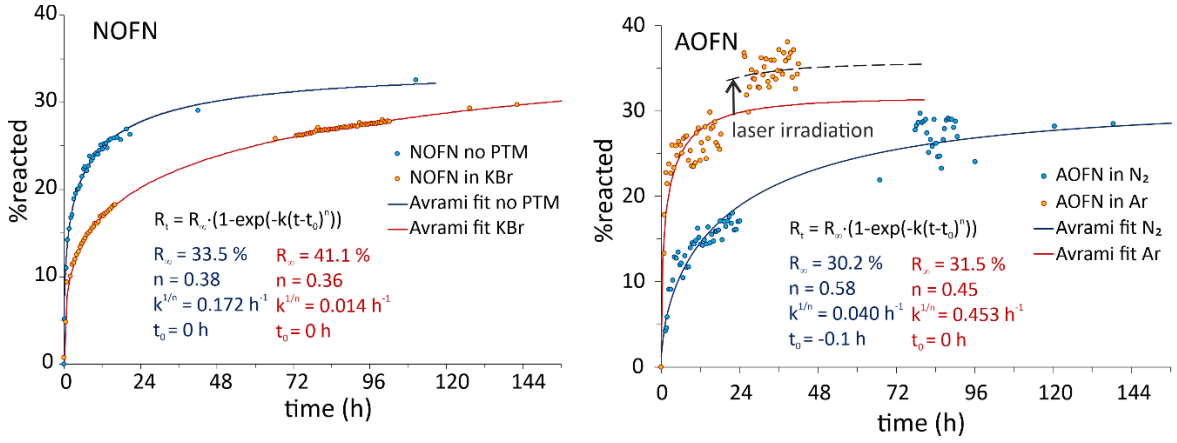

Figure 15. Kinetic curves representing the time evolution of (left) **NOFN** polymerization at 20.5 GPa (as a bulk material without PTM and in KBr PTM) and (right) **AOFN** polymerization at 25.5 GPa (in N_2) and 22 GPa (in Ar) and ambient temperature from the decrease of the integrated areas of the IR absorbance bands at 1745 cm^{-1} (**NOFN**), 820 cm^{-1} (**AOFN** in N_2), and 1550 cm^{-1} (**AOFN** in Ar), respectively. The fit to the modified Avrami equation (given in the plots) is represented by the solid lines. The data scatter is larger for **AOFN** due to higher uncertainties introduced by the overlap of IR mode tails.

While we intensively studied the reaction kinetics, we also observed the effects of PTM, pressure increase, or laser irradiation on the reaction. When **AOFN** was loaded with KBr as PTM, the reaction onset pressure was lower than with nitrogen or helium as the PTM. This led to overshooting of the onset pressure in this experiment and, hence, the chemical reaction was followed with a pressure increase up to 30.4 GPa on a short time scale instead of following its time dependence. We noticed a severe effect of pressure on the reaction leading to a largely reacted sample at the highest pressure (Figure 12). Furthermore, we observed a change of the sample color from colorless to orange. A change in **NOFN** color was also reported by Ward *et al.*[9] During the reaction of **NOFN** in nitrogen as the PTM, we noticed that irradiation of the partly reacted sample with a ca. 1 mW laser at 532 nm, which was used for pressure determination by the ruby fluorescence technique,[41] for just a few minutes greatly enhanced the reaction (Figure S21 in the Supporting Information). This is probably due to the effect of two-photon absorption induced reactivity, which is quite common in molecular compounds at high pressures due to the red shifts of the excited states; examples are benzene, water, and butadiene.[1a, 4k, 29a-c] The reaction can be triggered by only few excited molecules and then usually proceeds by itself in a condensation process. A closer investigation of this effect in **NOFN** and **AOFN** is the subject of future studies.[29d] In order to exclude this effect in our kinetic study, we performed a time-dependent reaction experiment on **NOFN**, in which the sample was

loaded as a bulk material without a PTM and without a ruby pressure standard (Figures 15 and S22). The pressure was calibrated via the pressure shift of the vibrational modes, as determined in the previous experiments, in order not to irradiate the sample.

CONCLUSIONS

To the best of our knowledge, this is the first time that the pressure evolution of the single crystal structure of aromatic compounds has been studied experimentally with high accuracy to a pressure close to the pressure of polymerization and thus loss of aromaticity (ca. 20 GPa), which is associated with the conversion of C–C π-bonds to inter-ring σ-bonds. From our experimental structural data on **NOFN** and **AOFN** we conclude that π–stacked molecules with a nn C···C distance of ca. 2.65–2.70 Å are still stable at high pressure. On further compression below this distance, chemical reactions will start. This is in agreement with the critical intermolecular C···C reaction distance of 2.6 Å (corrected for thermal uncertainty) previously reported from theoretical calculations on the structural compression of benzene,[1a] and also with the nn C···C distance of ca. 2.8 Å (with thermal uncertainty) between benzene and hexafluorobenzene at 20 GPa obtained from a powder neutron diffraction study.[8]

As reported in recent studies, the smallest arene-perfluoroarene co-crystal, namely 1:1 benzene:hexafluorobenzene, shows a complex high-pressure behavior with four pressure-induced phase transitions before polymerization to a proposed graphane-type polymer structure occurs at > 20–25 GPa.[2e, 8] In contrast, the 1:1 arene-perfluoroarene co-crystals of the larger molecules naphthalene and anthracene with octafluoronaphthalene show an extraordinarily stable stacking arrangement within the crystal structure up to the onset of pressure-induced polymerization at 21–25 GPa. This leads to the conclusion that the π–π arene–perfluoroarene interaction is stronger and more robust for the larger molecules, which have a larger surface area, possibly due to larger van der Waals (dispersion) interactions between the molecules. Hence, the simplest arene-perfluoroarene system does not seem to be the prototypical system for structural and high-pressure investigations, and is also not the most representative of the high-pressure behavior of arene-perfluoroarene co-crystals.

Our study on **NOFN** and **AOFN** shows that the arene-perfluoroarene interaction is a valuable synthon not only for generation of parallel π-stacking in 1:1 co-crystals of arenes and perfluoroarenes and interesting liquid-crystal phase behavior which indicates the persistence of these interactions at temperatures up to around 200 °C,[19a, 19k] but also for the stabilization of these stacked structures of polycyclic aromatic hydrocarbons (PAHs) and perfluoroarenes at

high pressure. The retention of the stacking arrangement has the advantage of formatting polymers with highly-ordered columns of hydrofluorocarbons by chemical reaction at pressures > 21 GPa. It is postulated here that stacks of more extended polycyclic aromatic hydrocarbons and fluorocarbons will provide a useful means to control the width and lateral extension of the columns.

ACKNOWLEDGMENTS

The authors thank the ESRF for synchrotron beamtime. Financial support from the ESRF and the Julius-Maximilians-Universität Würzburg is greatly appreciated. The research leading to these results has received funding from LASERLAB-EUROPE (grant agreement no. 654148, European Union's Horizon 2020 research and innovation programme). This work was supported by the Spanish Ministry of Science, Innovation and Universities under Grant MAT2016-75586-C4-1-P and by Generalitat Valenciana under Grant Prometeo/2018/123 (EFIMAT). J.R.-F. thanks the Spanish MICINN for project PGC2018-097520-A-100. Durham's Hamilton HPC service and the UK Archer supercomputer were used under grant EPSRC EP/P022782/1.

ASSOCIATED CONTENT

Details of crystal growth, experimental methods (single-crystal X-ray diffraction, infrared spectroscopy), and computational methods are included in the Supporting Information. This material is available free of charge via the Internet at http://pubs.acs.org.

AUTHOR INFORMATION

Corresponding Authors

Alexandra Friedrich — *Institut für Anorganische Chemie, Julius-Maximilians-Universität Würzburg, Am Hubland, 97074 Würzburg, Germany;* orcid.org/0000-0002-1411-7336; Email: alexandra.friedrich1@uni-wuerzburg.de

Roberto Bini — *LENS, European Laboratory for Nonlinear Spectroscopy, Via Nello Carrara 1, 50019 Sesto Fiorentino (FI), Italy; ICCOM-CNR, Institute of Chemistry of OrganoMetallic Compounds, National Research Council of Italy, Via Madonna del Piano 10, I-50019 Sesto Fiorentino, Firenze, Italy; Dipartimento di Chimica "Ugo Schiff"*

dell'Università degli Studi di Firenze, Via della Lastruccia 3, 50019 Sesto Fiorentino (FI), Italy; orcid.org/0000-0002-6746-696X; Email: roberto.bini@unifi.it

Stewart J. Clark — *Department of Physics, University of Durham, Science Labs, South Road, Durham DH1 3LE, UK*; orcid.org/0000-0003-4792-7738; Email: s.j.clark@durham.ac.uk

Todd B. Marder — *Institut für Anorganische Chemie, Julius-Maximilians-Universität Würzburg, Am Hubland, 97074 Würzburg, Germany*; orcid.org/0000-0002-9990-0169; Email: todd.marder@uni-wuerzburg.de

Authors

Ines E. Collings — *European Synchrotron Radiation Facility, 71 Avenue des Martyrs, 38000 Grenoble, France;* orcid.org/0000-0002-9851-2615

Kamil Dziubek — *LENS, European Laboratory for Nonlinear Spectroscopy, Via Nello Carrara 1, 50019 Sesto Fiorentino (FI), Italy;* orcid.org/0000-0001-7577-4527

Samuele Fanetti — *LENS, European Laboratory for Nonlinear Spectroscopy, Via Nello Carrara 1, 50019 Sesto Fiorentino (FI), Italy; ICCOM-CNR, Institute of Chemistry of OrganoMetallic Compounds, National Research Council of Italy, Via Madonna del Piano 10, I-50019 Sesto Fiorentino, Firenze, Italy;* orcid.org/0000-0002-5688-6272

Krzysztof Radacki — *Institut für Anorganische Chemie, Julius-Maximilians-Universität Würzburg, Am Hubland, 97074 Würzburg, Germany;* orcid.org/0000-0003-3088-6327

Javier Ruiz-Fuertes — *MALTA Consolider Team, Dpto. Física Aplicada-ICMUV, Universitat de València, C/ Doctor Moliner 50, 46100 Burjassot, Spain; DCITIMAC, MALTA Consolider Team, Universidad de Cantabria, 39005 Santander, Spain;* orcid.org/0000-0003-3175-7754

Julio Pellicer-Porres — *MALTA Consolider Team, Dpto. Física Aplicada-ICMUV, Universitat de València, C/ Doctor Moliner 50, 46100 Burjassot, Spain;* orcid.org/0000-0002-4288-900X

Michael Hanfland — *European Synchrotron Radiation Facility, 71 Avenue des Martyrs, 38000 Grenoble, France;* orcid.org/0000-0002-8904-5461

Daniel Sieh — *Institut für Anorganische Chemie, Julius-Maximilians-Universität Würzburg, Am Hubland, 97074 Würzburg, Germany;*

Present Addresses

Ines E. Collings — *Center of X-ray Analytics, Empa – Swiss Federal Laboratories for Materials Science and Technology, Überlandstraße 129, 8600 Dübendorf, Switzerland*

Notes

The authors declare no competing financial interest.

REFERENCES

1. (a) Ciabini, L.; Santoro, M.; Gorelli, F. A.; Bini, R.; Schettino, V.; Raugei, S. Triggering dynamics of the high-pressure benzene amorphization. *Nat. Mater.* **2007,** *6*, 39-43. (b) Fitzgibbons, T. C.; Guthrie, M.; Xu, E. S.; Crespi, V. H.; Davidowski, S. K.; Cody, G. D.; Alem, N.; Badding, J. V. Benzene-derived carbon nanothreads. *Nat. Mater.* **2015,** *14*, 43-47. (c) Klier, K.; Landskron, K. Thermodynamically Controlled High-Pressure High-Temperature Synthesis of Crystalline Fluorinated sp^3-Carbon Networks. *J. Phys. Chem. C* **2015,** *119*, 26086-26090.
2. (a) Drickamer, H. G. Pi Electron Systems at High Pressure. *Science* **1967,** *156*, 1183-1189. (b) Engelke, R.; Blais, N. C. Chemical dimerization of crystalline anthracene produced by transient high pressure. *J. Chem. Phys.* **1994,** *101*, 10961-10972. (c) Shinozaki, A.; Mimura, K.; Nishida, T.; Inoue, T.; Nakano, S.; Kagi, H. Stability and partial oligomerization of naphthalene under high pressure at room temperature. *Chem. Phys. Lett.* **2016,** *662*, 263-267. (d) Cai, W. Z.; Zhang, R.; Yao, Y. S.; Deemyad, S. Piezochromism and structural and electronic properties of benz[*a*]anthracene under pressure. *Phys. Chem. Chem. Phys.* **2017,** *19*, 6216-6223. (e) Wang, Y. J.; Wang, L. J.; Zheng, H. Y.; Li, K.; Andrzejewski, M.; Hattori, T.; Sano-Furukawa, A.; Katrusiak, A.; Meng, Y. F.; Liao, F. H.; Hong, F.; Mao, H. K. Phase Transitions and Polymerization of C_6H_6-C_6F_6 Cocrystal under Extreme Conditions. *J. Phys. Chem. C* **2016,** *120*, 29510-29519. (f) Pruzan, P.; Chervin, J. C.; Thiery, M. M.; Itie, J. P.; Besson, J. M.; Forgerit, J. P.; Revault, M. Transformation of benzene to a polymer after static pressurization to 30 GPa. *J. Chem. Phys.* **1990,** *92*, 6910-6915.
3. (a) Warnes, R. H. Shock Wave Compression of Three Polynuclear Aromatic Compounds. *J. Chem. Phys.* **1970,** *53*, 1088-1094. (b) Aust, R. B.; Drickamer, H. G.; Bentley, W. H. Behavior of Fused-Ring Aromatic Hydrocarbons at Very High Pressure. *J. Chem. Phys.* **1964,** *41*, 1856-1864.

4. (a) Thiery, M. M.; Leger, J. M. High pressure solid phases of benzene. 1. Raman and x-ray studies of C_6H_6 at 294 K up to 25 GPa. *J. Chem. Phys.* **1988,** *89*, 4255-4271. (b) Silveira, J.; Muniz, A. R. Functionalized diamond nanothreads from benzene derivatives. *Phys. Chem. Chem. Phys.* **2017,** *19*, 7132-7137. (c) Engelke, R.; Hay, P. J.; Kleier, D. A.; Wadt, W. R. A theoretical study of possible benzene dimerizations under high-pressure conditions. *J. Chem. Phys.* **1983,** *79*, 4367-4375. (d) Ciabini, L.; Gorelli, F. A.; Santoro, M.; Bini, R.; Schettino, V.; Mezouar, M. High-pressure and high-temperature equation of state and phase diagram of solid benzene. *Phys. Rev. B* **2005,** *72*, 094108. (e) Ciabini, L.; Santoro, M.; Bini, R.; Schettino, V. High pressure photoinduced ring opening of benzene. *Phys. Rev. Lett.* **2002,** *88*, 085505. (f) Ciabini, L.; Santoro, M.; Bini, R.; Schettino, V. High pressure reactivity of solid benzene probed by infrared spectroscopy. *J. Chem. Phys.* **2002,** *116*, 2928-2935. (g) Ciabini, L.; Santoro, M.; Bini, R.; Schettino, V. High pressure crystal phases of benzene probed by infrared spectroscopy. *J. Chem. Phys.* **2001,** *115*, 3742-3749. (h) Jackson, B. R.; Trout, C. C.; Badding, J. V. UV Raman analysis of the C:H network formed by compression of benzene. *Chem. Mater.* **2003,** *15*, 1820-1824. (i) Budzianowski, A.; Katrusiak, A. Pressure-frozen benzene I revisited. *Acta Crystallogr. Sect. B: Struct. Sci.* **2006,** *62*, 94-101. (j) Katrusiak, A.; Podsiadlo, M.; Budzianowski, A. Association CH···π and No van der Waals Contacts at the Lowest Limits of Crystalline Benzene I and II Stability Regions. *Cryst. Growth Des.* **2010,** *10*, 3461-3465. (k) Citroni, M.; Bini, R.; Foggi, P.; Schettino, V. Role of excited electronic states in the high-pressure amorphization of benzene. *Proc. Natl. Acad. Sci. U.S.A.* **2008,** *105*, 7658-7663. (l) Wen, X. D.; Hoffmann, R.; Ashcroft, N. W. Benzene under High Pressure: a Story of Molecular Crystals Transforming to Saturated Networks, with a Possible Intermediate Metallic Phase. *J. Am. Chem. Soc.* **2011,** *133*, 9023-9035. (m) He, C. Y.; Sun, L. Z.; Zhang, C. X.; Zhong, J. X. Low energy three-dimensional hydrocarbon crystal from cold compression of benzene. *J. Phys.: Condens. Matter* **2013,** *25*, 205403. (n) Shinozaki, A.; Mimura, K.; Kagi, H.; Komatu, K.; Noguchi, N.; Gotou, H. Pressure-induced oligomerization of benzene at room temperature as a precursory reaction of amorphization. *J. Chem. Phys.* **2014,** *141*, 084306. (o) Chen, B.; Hoffmann, R.; Ashcroft, N. W.; Badding, J.; Xu, E. S.; Crespi, V. Linearly Polymerized Benzene Arrays As Intermediates, Tracing Pathways to Carbon Nanothreads. *J. Am. Chem. Soc.* **2015,** *137*, 14373-14386. (p) Li, X.; Baldin, M.; Wang, T.; Chen, B.; Xu, E. S.; Vermilyea, B.; Crespi, V. H.; Hoffmann, R.; Molaison, J. J.; Tulk, C. A.; Guthrie, M.; Sinogeikin, S.; Badding, J. V.

Mechanochemical Synthesis of Carbon Nanothread Single Crystals. *J. Am. Chem. Soc.* **2017,** *139*, 16343-16349. (q) Chanyshev, A. D.; Litasov, K. D.; Rashchenko, S. V.; Sano-Furukawa, A.; Kagi, H.; Hattori, T.; Shatskiy, A. F.; Dymshits, A. M.; Sharygin, I. S.; Higo, Y. High-Pressure-High-Temperature Study of Benzene: Refined Crystal Structure and New Phase Diagram up to 8 GPa and 923 K. *Cryst. Growth Des.* **2018,** *18*, 3016-3026. (r) Duan, P.; Li, X.; Wang, T.; Chen, B.; Juhl, S. J.; Koeplinger, D.; Crespi, V. H.; Badding, J. V.; Schmidt-Rohr, K. The Chemical Structure of Carbon Nanothreads Analyzed by Advanced Solid-State NMR. *J. Am. Chem. Soc.* **2018,** *140*, 7658-7666. (s) Wang, T.; Duan, P.; Xu, E. S.; Vermilyea, B.; Chen, B.; Li, X.; Badding, J. V.; Schmidt-Rohr, K.; Crespi, V. H. Constraining Carbon Nanothread Structures by Experimental and Calculated Nuclear Magnetic Resonance Spectra. *Nano Lett.* **2018,** *18*, 4934-4942. (t) Juhl, S. J.; Wang, T.; Vermilyea, B.; Li, X.; Crespi, V. H.; Badding, J. V.; Alem, N. Local Structure and Bonding of Carbon Nanothreads Probed by High-Resolution Transmission Electron Microscopy. *J. Am. Chem. Soc.* **2019,** *141*, 6937-6945.

5. Oehzelt, M.; Resel, R.; Hummer, K.; Puschnig, P.; Ambrosch-Draxl, C.; Nakayama, A. X-ray diffraction study of anthracene under high pressure. *Synth. Met.* **2003,** *137*, 913-914.

6. (a) Cammi, R. A New Extension of the Polarizable Continuum Model: Toward a Quantum Chemical Description of Chemical Reactions at Extreme High Pressure. *J. Comput. Chem.* **2015,** *36*, 2246-2259. (b) Chen, B.; Wang, T.; Crespi, V. H.; Li, X.; Badding, J.; Hoffmann, R. All the Ways To Have Substituted Nanothreads. *J. Chem. Theory Comput.* **2018,** *14*, 1131-1140. (c) Demingos, P. G.; Muniz, A. R. Carbon nanothreads from polycyclic aromatic hydrocarbon molecules. *Carbon* **2018,** *140*, 644-652.

7. (a) Nobrega, M. M.; Teixeira-Neto, E.; Cairns, A. B.; Temperini, M. L. A.; Bini, R. One-dimensional diamondoid polyaniline-like nanothreads from compressed crystal aniline. *Chem. Sci.* **2018,** *9*, 254-260. (b) Li, X.; Wang, T.; Duan, P.; Baldini, M.; Huang, H. T.; Chen, B.; Juhl, S. J.; Koeplinger, D.; Crespi, V. H.; Schmidt-Rohr, K.; Hoffmann, R.; Alem, N.; Guthrie, M.; Zhang, X.; Badding, J. V. Carbon Nitride Nanothread Crystals Derived from Pyridine. *J. Am. Chem. Soc.* **2018,** *140*, 4969-4972. (c) Fanetti, S.; Santoro, M.; Alabarse, F.; Enrico, B.; Bini, R. Modulating the H-bond strength by varying the temperature for the high pressure synthesis of nitrogen rich carbon nanothreads. *Nanoscale* **2020,** *12*, 5233-5242.

8. Wang, Y. J.; Dong, X.; Tang, X. Y.; Zheng, H. Y.; Li, K.; Lin, X. H.; Fang, L. M.; Sun, G. A.; Chen, X. P.; Xie, L.; Bull, C. L.; Funnell, N. P.; Hattori, T.; Sano-Furukawa, A.; Chen, J. H.; Hensley, D. K.; Cody, G. D.; Ren, Y.; Lee, H. H.; Mao, H. K. Pressure-Induced Diels-Alder Reactions in C_6H_6-C_6F_6 Cocrystal towards Graphane Structure. *Angew. Chem. Int. Ed.* **2019,** *58*, 1468-1473.

9. Ward, M. D.; Tang, W. S.; Zhu, L.; Popov, D.; Cody, G. D.; Strobel, T. A. Controlled Single-Crystalline Polymerization of $C_{10}H_8 \cdot C_{10}F_8$ under Pressure. *Macromolecules* **2019,** *52*, 7557-7563.

10. Capitani, F.; Hoppner, M.; Malavasi, L.; Marini, C.; Artioli, G. A.; Hanfland, M.; Dore, P.; Boeri, L.; Postorino, P. Structural Evolution of Solid Phenanthrene at High Pressures. *J. Phys. Chem. C* **2016,** *120*, 14310-14316.

11. (a) Citroni, M.; Fanetti, S.; Bazzicalupi, C.; Dziubek, K.; Pagliai, M.; Nobrega, M. M.; Mezouar, M.; Bini, R. Structural and Electronic Competing Mechanisms in the Formation of Amorphous Carbon Nitride by Compressing *s*-Triazine. *J. Phys. Chem. C* **2015,** *119*, 28560-28569. (b) Fanetti, S.; Nobrega, M. M.; Teixeira-Neto, E.; Temperini, M. L. A.; Bini, R. Effect of Structural Anisotropy in High-Pressure Reaction of Aniline. *J. Phys. Chem. C* **2018,** *122*, 29158-29164.

12. Shelton, H.; Dera, P.; Tkachev, S. Evolution of Interatomic and Intermolecular Interactions and Polymorphism of Melamine at High Pressure. *Crystals* **2018,** *8*, 265.

13. Collings, I. E.; Hanfland, M. Packing Rearrangements in 4-Hydroxycyanobenzene Under Pressure. *Molecules* **2019,** *24*, 1759.

14. Casati, N.; Kleppe, A.; Jephcoat, A. P.; Macchi, P. Putting pressure on aromaticity along with *in situ* experimental electron density of a molecular crystal. *Nat. Commun.* **2016,** *7*, 10901.

15. (a) Clark, S. J.; Segall, M. D.; Pickard, C. J.; Hasnip, P. J.; Probert, M. J.; Refson, K.; Payne, M. C. First principles methods using CASTEP. *Z. Kristallogr.* **2005,** *220*, 567-570. (b) Segall, M. D.; Lindan, P. J. D.; Probert, M. J.; Pickard, C. J.; Hasnip, P. J.; Clark, S. J.; Payne, M. C. First-principles simulation: ideas, illustrations and the CASTEP code. *J. Phys.: Condens. Matter* **2002,** *14*, 2717-2744.

16. (a) Dahl, T. Crystallographic Studies of Molecular Complexes Containing Hexafluorobenzene. *Acta Chem. Scand.* **1988,** *42*, 1-7. (b) Coates, G. W.; Dunn, A. R.; Henling, L. M.; Dougherty, D. A.; Grubbs, R. H. Phenyl-perfluorophenyl stacking interactions: A new strategy for supermolecule construction. *Angew. Chem. Int. Ed. Engl.* **1997,** *36*, 248-251. (c) West, A. P.; Mecozzi, S.; Dougherty, D. A. Theoretical

studies of the supramolecular synthon benzene···hexafluorobenzene. *J. Phys.Org. Chem.* **1997,** *10*, 347-350. (d) Collings, J. C.; Roscoe, K. P.; Thomas, R. L.; Batsanov, A. S.; Stimson, L. M.; Howard, J. A. K.; Marder, T. B. Arene-perfluoroarene interactions in crystal engineering. Part 3. Single-crystal structures of 1 : 1 complexes of octafluoronaphthalene with fused-ring polyaromatic hydrocarbons. *New J. Chem.* **2001,** *25*, 1410-1417.

17. Williams, J. H. The Molecular Electric Quadrupole-Moment and Solid-State Architecture. *Acc. Chem. Res.* **1993,** *26*, 593-598.

18. Patrick, C. R.; Prosser, G. S. Molecular Complex of Benzene and Hexafluorobenzene. *Nature* **1960,** *187*, 1021-1021.

19. (a) Dai, C.; Nguyen, P.; B. Marder, T.; B. Marder, T.; J. Scott, A.; Clegg, W.; Viney, C.; Viney, C. Control of single crystal structure and liquid crystal phase behaviour via arene-perfluoroarene interactions. *Chem. Commun.* **1999**, 2493-2494. (b) Batsanov, A. S.; Collings, J. C.; Howard, J. A. K.; Marder, T. B.; Perepichka, D. F. Arene-perfluoroarene interactions in crystal engineering. 5. Octafluoronaphthalene-tetrathiafulvalene (1/1). *Acta Crystallogr. C* **2001,** *57*, 1306-1307. (c) Batsanov, A. S.; Collings, J. C.; Howard, J. A. K.; Marder, T. B. Octafluoronaphthalene-1,8-diaminonaphthalene (1/1). *Acta Crystallogr. E* **2001,** *57*, o950-o952. (d) Collings, J. C.; Batsanov, A. S.; Howard, J. A. K.; Marder, T. B. Octafluoronaphthalene-diphenylacetylene (1/1). *Acta Crystallogr. C* **2001,** *57*, 870-872. (e) Batsanov, A. S.; Howard, J. A. K.; Marder, T. B.; Robins, E. G. Arene-perfluoroarene interactions in crystal engineering. 4. Hexafluorobenzene-trans-stilbene (1/1). *Acta Crystallogr. C* **2001,** *57*, 1303-1305. (f) Collings, J. C.; Batsanov, A. S.; Howard, J. A. K.; Marder, T. B. Arene-perfluoroarene interactions in crystal engineering 7: single-crystal structures of 1:1 complexes of octafluoronaphthalene and hexafluorobenzene with acenaphthene. *Cryst. Eng.* **2002,** *5*, 37-46. (g) Collings, J. C.; Roscoe, K. P.; Robins, E. G.; Batsanov, A. S.; Stimson, L. M.; Howard, J. A. K.; Clark, S. J.; Marder, T. B. Arene-perfluoroarene interactions in crystal engineering 8: structures of 1 : 1 complexes of hexafluorobenzene with fused-ring polyaromatic hydrocarbons. *New. J. Chem.* **2002,** *26*, 1740-1746. (h) Smith, C. E.; Smith, P. S.; Thomas, R. L.; Robins, E. G.; Collings, J. C.; Dai, C. Y.; Scott, A. J.; Borwick, S.; Batsanov, A. S.; Watt, S. W.; Clark, S. J.; Viney, C.; Howard, J. A. K.; Clegg, W.; Marder, T. B. Arene-perfluoroarene interactions in crystal engineering: structural preferences in polyfluorinated tolans. *J. Mater. Chem.* **2004,** *14*, 413-420. (i) Collings, J. C.; Smith, P. S.; Yufit, D. S.; Batsanov, A. S.; Howard, J. A.

K.; Marder, T. B. Arene-perfluoroarene interactions in crystal engineering. Part 10. Crystal structures of 1 : 1 complexes of octafluoronaphthalene with biphenyl and biphenylene. *CrystEngComm* **2004,** *6*, 25-28. (j) Collings, J. C.; Burke, J. M.; Smith, P. S.; Batsanov, A. S.; Howard, J. A. K.; Marder, T. B. The synthesis and crystal structures of halogenated tolans *p*-X-C_6H_4-C≡C-C_6F_5 and *p*-X-C_6F_4-C≡C-C_6H_5 (X = F, Cl, Br, I). *Org. Biomol. Chem.* **2004,** *2*, 3172-3178. (k) Watt, S. W.; Dai, C.; Scott, A. J.; Burke, J. M.; Thomas, R. L.; Collings, J. C.; Viney, C.; Clegg, W.; Marder, T. B. Structure and Phase Behavior of a 2:1 Complex between Arene- and Fluoroarene-Based Conjugated Rigid Rods. *Angew. Chem. Int. Ed.* **2004,** *43*, 3061-3063. (l) Fasina, T. M.; Collings, J. C.; Lydon, D. P.; Albesa-Jove, D.; Batsanov, A. S.; Howard, J. A. K.; Nguyen, P.; Bruce, M.; Scott, A. J.; Clegg, W.; Watt, S. W.; Viney, C.; Marder, T. B. Synthesis, optical properties, crystal structures and phase behaviour of selectively fluorinated 1,4-bis(4'-pyridylethynyl)benzenes, 4-(phenylethynyl)pyridines and 9,10-bis(4'-pyridylethynyl)anthracene, and a $Zn(NO_3)_2$ coordination polymer. *J. Mater. Chem.* **2004,** *14*, 2395-2404. (m) Fasina, T. M.; Collings, J. C.; Burke, J. M.; Batsanov, A. S.; Ward, R. M.; Albesa-Jove, D.; Porres, L.; Beeby, A.; Howard, J. A. K.; Scott, A. J.; Clegg, W.; Watt, S. W.; Viney, C.; Marder, T. B. Synthesis, optical properties, crystal structures and phase behaviour of symmetric, conjugated ethynylarene-based rigid rods with terminal carboxylate groups. *J. Mater. Chem.* **2005,** *15*, 690-697. (n) Collings, J. C.; Batsanov, A. S.; Howard, J. A. K.; Dickie, D. A.; Clyburne, J. A. C.; Jenkins, H. A.; Marder, T. B. 1 : 1 Complexes of octafluoronaphthalene with trans-stilbene and trans-azobenzene. *J. Fluorine Chem.* **2005,** *126*, 515-519. (o) Collings, J. C.; Batsanov, A. S.; Howard, J. A. K.; Marder, T. B. Arene-perfluoroarene interactions in crystal engineering. Part 14. 1:1 Complexes of octafluoronaphthalene with fluorene and 9,10-dihydrophenanthrene. *Can. J. Chem.* **2006,** *84*, 238-242. (p) Batsanov, A. S.; Mkhalid, I. A. I.; Marder, T. B. 4,4'-di-*tert*-butyl-2,2'-bipyridine-hexafluorobenzene (1/1). *Acta Crystallogr. E* **2007,** *63*, o1196-o1198. (q) Batsanov, A. S.; Howard, J. A. K.; Albesa-Jove, D.; Collings, J. C.; Liu, Z. Q.; Mkhalid, I. A. I.; Thibault, M. H.; Marder, T. B. Structural Versatility of Pyrene-2-(4,4,5,5-tetramethyl-[1,3,2]dioxaborolane) and Pyrene-2,7-bis(4,4,5,5-tetramethyl-[1,3,2]dioxaborolane). *Cryst. Growth Des.* **2012,** *12*, 2794-2802.

20. (a) Chen, H.; Ni, B. B.; Gao, F.; Ma, Y. G. Pressure-accelerated copper-free cycloaddition of azide and alkyne groups pre-organized in the crystalline state at room temperature. *Green Chem.* **2012,** *14*, 2703-2705. (b) Ni, B. B.; Wang, K.; Yan, Q. F.;

Chen, H.; Ma, Y. G.; Zou, B. Pressure accelerated 1,3-dipolar cycloaddition of azide and alkyne groups in crystals. *Chem. Commun.* **2013,** *49*, 10130-10132.

21. Desgreniers, S.; Kourouklis, G. A.; Jayaraman, A.; Kaplan, M. L.; Schmidt, P. H. A Raman spectroscopic study of naphthalene:octafluoronaphthalene at high pressure and low temperature. *J. Chem. Phys.* **1985,** *83*, 480-485.
22. Li, W. B.; Duan, D. F.; Huang, X. L.; Jin, X. L.; Yang, X.; Li, S. R.; Jiang, S. Q.; Huang, Y. P.; Li, F. F.; Cui, Q. L.; Zhou, Q.; Liu, B. B.; Cui, T. Pressure-Induced Diversity of π-Stacking Motifs and Amorphous Polymerization in Pyrrole. *J. Phys. Chem. C* **2014,** *118*, 12420-12427.
23. Pravica, M.; Sneed, D.; Wang, Y. G.; Smith, Q.; White, M. Hexafluorobenzene under Extreme Conditions. *J. Phys. Chem. B* **2016,** *120*, 2854-2858.
24. Further NMR spectroscopy and high-resolution mass spectrometry analyses of the polymerized products were prevented due to the small sample sizes obtained from the high-pressure experiments and the insolubility of the polymerized samples. Based on the results obtained in this study we plan to work with bulk samples in our future studies on these and related compounds.
25. Vaidya, S. N.; Kennedy, G. C. Compressibility of 18 Molecular Organic Solids to 45 kbar. *J. Chem. Phys.* **1971,** *55*, 987-992.
26. Klotz, S.; Chervin, J. C.; Munsch, P.; Le Marchand, G. Hydrostatic limits of 11 pressure transmitting media. *J. Phys. D: Appl. Phys.* **2009,** *42*, 075413.
27. (a) Vinet, P.; Ferrante, J.; Smith, J. R.; Rose, J. H. A universal equation of state for solids. *J. Phys. C: Solid State Phys.* **1986,** *19*, L467-L473. (b) Vinet, P.; Rose, J. H.; Ferrante, J.; Smith, J. R. Universal features of the equation of state of solids. *J. Phys.: Condens. Matter* **1989,** *1*, 1941-1963.
28. Lejaeghere, K.; Bihlmayer, G.; Bjorkman, T.; Blaha, P.; Blugel, S.; Blum, V.; Caliste, D.; Castelli, I. E.; Clark, S. J.; Dal Corso, A.; de Gironcoli, S.; Deutsch, T.; Dewhurst, J. K.; Di Marco, I.; Draxl, C.; Dulak, M.; Eriksson, O.; Flores-Livas, J. A.; Garrity, K. F.; Genovese, L.; Giannozzi, P.; Giantomassi, M.; Goedecker, S.; Gonze, X.; Granas, O.; Gross, E. K. U.; Gulans, A.; Gygi, F.; Hamann, D. R.; Hasnip, P. J.; Holzwarth, N. A. W.; Iusan, D.; Jochym, D. B.; Jollet, F.; Jones, D.; Kresse, G.; Koepernik, K.; Kucukbenli, E.; Kvashnin, Y. O.; Locht, I. L. M.; Lubeck, S.; Marsman, M.; Marzari, N.; Nitzsche, U.; Nordstrom, L.; Ozaki, T.; Paulatto, L.; Pickard, C. J.; Poelmans, W.; Probert, M. I. J.; Refson, K.; Richter, M.; Rignanese, G. M.; Saha, S.; Scheffler, M.; Schlipf, M.; Schwarz, K.; Sharma, S.; Tavazza, F.; Thunstrom, P.; Tkatchenko, A.;

Torrent, M.; Vanderbilt, D.; van Setten, M. J.; Van Speybroeck, V.; Wills, J. M.; Yates, J. R.; Zhang, G. X.; Cottenier, S. Reproducibility in density functional theory calculations of solids. *Science* **2016,** *351*, 1415.

29. (a) Citroni, M.; Ceppatelli, M.; Bini, R.; Schettino, V. Laser-induced selectivity for dimerization versus polymerization of butadiene under pressure. *Science* **2002,** *295*, 2058-2060. (b) Bini, R. Laser-assisted high-pressure chemical reactions. *Acc. Chem. Res.* **2004,** *37*, 95-101. (c) Ceppatelli, M.; Bini, R.; Schettino, V. High-pressure photodissociation of water as a tool for hydrogen synthesis and fundamental chemistry. *Proc. Natl. Acad. Sci. U.S.A.* **2009,** *106*, 11454-11459. (d) While studies of the two-photon absorption induced polymerization process for this sample are beyond the scope of the current manuscript, such detailed studies are in progress and will be reported in due course.
30. Potenza, J.; Mastropaolo, D. Naphthalene-Octafluoronaphthalene, 1:1 Solid Compound. *Acta Crystallogr. B* **1975,** *31*, 2527-2529.
31. (a) Hunter, C. A.; Sanders, J. K. M. The Nature of π-π Interactions. *J. Am. Chem. Soc.* **1990,** *112*, 5525-5534. (b) Loots, L.; Barbour, L. J. A Rudimentary Method for Classification of π···π Packing Motifs for Aromatic Molecules. In *Pi-Interaction in Crystal Engineering: Frontiers in Crystal Engineering*, John Wiley & Sons: Chichester, UK, 2012; pp 109-124. (c) Dahl, T. The Nature of Stacking Interactions between Organic Molecules Elucidated by Analysis of Crystal Structures. *Acta Chem. Scand.* **1994,** *48*, 95-106.
32. Hammouri, M.; Garcia, T. M.; Cook, C.; Monaco, S.; Jezowski, S.; Marom, N.; Schatschneider, B. High-Throughput Pressure-Dependent Density Functional Theory Investigation of Herringbone Polycyclic Aromatic Hydrocarbons: Part 1. Pressure-Dependent Structure Trends. *J. Phys. Chem. C* **2018,** *122*, 23815-23827.
33. Casati, N.; Genoni, A.; Meyer, B.; Krawczuk, A.; Macchi, P. Exploring charge density analysis in crystals at high pressure: data collection, data analysis and advanced modelling. *Acta Crystallogr. Sect. B: Struct. Sci.* **2017,** *73*, 584-597.
34. Dahl, J. E.; Liu, S. G.; Carlson, R. M. K. Isolation and structure of higher diamondoids, nanometer-sized diamond molecules. *Science* **2003,** *299*, 96-99.
35. Günzler, H.; Heise, H. M. *IR-Spektroksopie: eine Einführung*. 3rd edition ed.; VCH Verlagsgesellschaft mbH: Weinheim, Germany, 1996.
36. Refson, K.; Tulip, P. R.; Clark, S. J. Variational density-functional perturbation theory for dielectrics and lattice dynamics. *Phys. Rev. B* **2006,** *73*, 155114.

37. Hudgins, D. M.; Sandford, S. A. Infrared spectroscopy of matrix isolated polycyclic aromatic hydrocarbons. 1. PAHs containing two to four rings. *J. Phys. Chem. A* **1998,** *102*, 329-343.

38. Schettino, V.; Bini, R. Molecules under extreme conditions: Chemical reactions at high pressure. *Phys. Chem. Chem. Phys.* **2003,** *5*, 1951-1965.

39. (a) Avrami, M. Granulation, phase change, and microstructure kinetics of phase change. III. *J. Chem. Phys.* **1941,** *9*, 177-184. (b) Avrami, M. Kinetics of phase change. II Transformation-time relations for random distribution of nuclei. *J. Chem. Phys.* **1940,** *8*, 212-224. (c) Avrami, M. Kinetics of phase change. I General theory. *J. Chem. Phys.* **1939,** *7*, 1103-1112.

40. Hulbert, S. F. Models for solid-state reactions in powdered compacts: A review. *J. Brit. Ceram. Soc.* **1969,** *6*, 11-20.

41. Mao, H. K.; Xu, J.; Bell, P. M. Calibration of the ruby pressure gauge to 800 kbar under quasi-hydrostatic conditions. *J. Geophys. Res.: Solid Earth* **1986,** *91*, 4673-4676.

42. Zhao, J.; Ross, N. L. Non-hydrostatic behavior of KBr as a pressure medium in diamond anvil cells up to 5.63 GPa. *J. Phys.: Condens. Matter* **2015,** *27*, 8.

TOC graphic

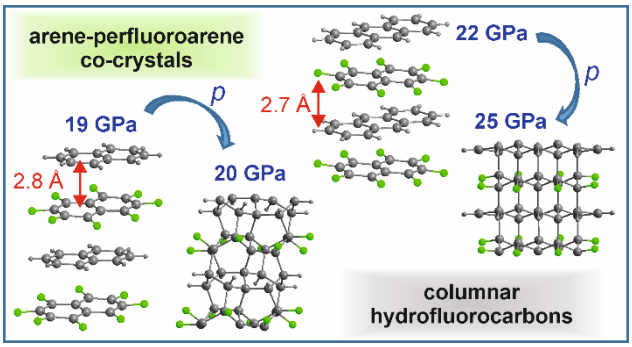
arene-perfluoroarene
co-crystals
19 GPa
p
20 GPa
2.8 Å
2.7 Å
22 GPa
p
25 GPa
columnar
hydrofluorocarbons